

(2) LEVEL II

AFRPL-TR-79-17

AN EXPERIMENTAL APPARATUS FOR INVESTIGATING
THE KINETIC REACTIONS IN SOLID ROCKET NOZZLES

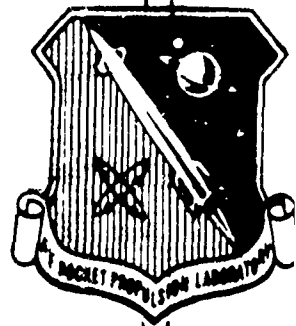
TECHNICAL REPORT

SCIENCE APPLICATIONS, INC.
18872 BARDEEN
IRVINE, CALIF. 92715

AUTHORS: J.P. Pope
R.B. Dirling

June 1979

APPROVED FOR PUBLIC RELEASE:
DISTRIBUTION UNLIMITED



AD A 071 318

DDC FILE COPY

DDC
RECEIVED
JUL 17 1979
B

Prepared for:

AIR FORCE ROCKET PROPULSION LABORATORY
DIRECTOR OF SCIENCE AND TECHNOLOGY
AIR FORCE SYSTEMS COMMAND
EDWARDS AFB, CALIFORNIA 93523

NOTICES

"When U.S. Government drawings, specifications, or other data are used for any purpose other than a definitely related Government procurement operation, the Government thereby incurs no responsibility nor any obligation whatsoever, and the fact that the Government may have formulated, furnished, or in any way supplied the said drawings, specifications or other data, is not to be regarded by implication or otherwise, as in any manner licensing the holder or any other person or corporation, or conveying any rights or permission to manufacture, use, or sell any patented invention that may in any way be related thereto."

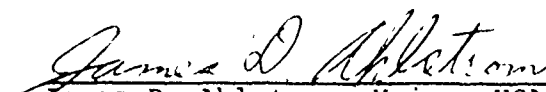
FOREWORD

This final report documents the results of a design, and manufacturing study performed by the Material Sciences Operation (MSO) of Science Applications, Incorporated (SAI) for the Air Force Rocket Propulsion Laboratory (AFRPL) under Contract FO4611-77-C-0047, Job Order Number 2307M2GS. The AFRPL Project Engineer was Lt C. R. Nelson II (AFRPL/MKBB). The SAI/MSO Project Manager was Mr. K. M. Kratsch and the Principal Investigator was Mr. J. P. Pope.

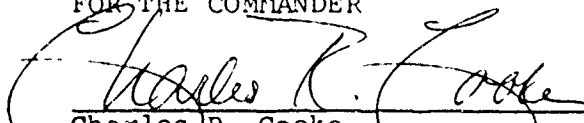
The design study of this program was accomplished at SAI/MSO with the manufacture of the components and pressure vessel for a Kinetic Test Cell subcontracted under purchase order to Algo Tool and Die, Santa Ana, California. Installation of the Kinetic Test Cell at the AFRPL was a joint effort of AFRPL and SAI/MSO personnel. Preparation of a laboratory test facility for integration of the Kinetic Test Cell was performed by AFRPL and grateful acknowledgment is extended to Lt Nelson and Mr. Leon Triplett for their cooperation and assistance.

This report has been reviewed by the Information Office/XOJ and is releasable to the National Technical Information Service (NTIS). At NTIS it will be available to the general public, including foreign nations. This technical report has been reviewed and is approved for publication; it is unclassified and suitable for general public release.


Charles R. Nelson II, 1Lt, USAF
Program Manager


James D. Ahlstrom, Major, USAF
Chief, Ballistic Missile and
Space Propulsion Branch


FOR THE COMMANDER


Charles R. Cooke
Director, Solid Rocket Division

REPORT DOCUMENTATION PAGE		READ INSTRUCTIONS BEFORE COMPLETING FORM
1. REPORT NUMBER (18) AFRPL TR-79-17	2. GOVT ACCESSION NO.	3. RECIPIENT'S CATALOG NUMBER (7)
4. TITLE (and Subtitle) (6) AN EXPERIMENTAL APPARATUS FOR INVESTIGATING THE KINETIC REACTIONS IN SOLID ROCKET NOZZLES		5. FUNDING NUMBERS Final Report. 2 Jun 77 - 30 Mar 79
7. AUTHOR(s) (10) J.P. Pope R.B. Dirling		8. CONTRACT OR GRANT NUMBER(s) (15) F04611-77-C-0047
9. PERFORMING ORGANIZATION NAME AND ADDRESS Science Applications Inc. P. O. Box 2351 1200 Prospect Street La Jolla, Ca. 92037		10. PROGRAM ELEMENT, PROJECT, TASK AREA & WORK UNIT NUMBERS Program Element 61102F Project 2307 JON:2307M2GS
11. CONTROLLING OFFICE NAME AND ADDRESS Air Force Rocket Propulsion Laboratory (AFSC) Edwards AFB CA 93523 MKBB		12. REPORT DATE (11) June 79
14. MONITORING AGENCY NAME & ADDRESS (if different from Controlling Office) (16) 5-1		13. NUMBER OF PAGES
15. SECURITY CLASS. (of this report) UNCLASSIFIED		15a. DECLASSIFICATION/DOWNGRADING SCHEDULE
16. DISTRIBUTION STATEMENT (of this Report) APPROVED FOR PUBLIC RELEASE; DISTRIBUTION UNLIMITED. (12) 62p (17) 112		
17. DISTRIBUTION STATEMENT (of the abstract entered in Block 20, if different from Report)		
18. SUPPLEMENTARY NOTES		
19. KEY WORDS (Continue on reverse side if necessary and identify by block number) Solid Rocket Nozzles Kinetic Reactions Carbon Carbon Materials Nozzle Recession		
20. ABSTRACT (Continue on reverse side if necessary and identify by block number) The present interest in carbon composite and bulk polycrystalline graphite materials for solid propellant rocket nozzles has occurred primarily due to the poor thermostructural performance of conventional pyrolytic graphite throat inserts as propellant flame temperature is increased. Circumvention of this problem has necessitated complex, multi-component nozzle configurations which are not only costly to fabricate but inherently less reliable than an integral design. Composite materials, in particular carbon-carbon composites, offer the potential of considerable improvement in manufacturing, reliability		

UNCLASSIFIED

SECURITY CLASSIFICATION OF THIS PAGE(When Data Entered)

and performance attributes compared to pyrolytic graphite. However, their ablation response in the primarily rate-controlled ablation regime of rocket nozzles is poorly understood. At the present time their ablation response is being assessed using the same techniques previously applied to non-porous pyrolytic graphite; e.g., evaluation of the kinetic coefficients from measurements of recession rate in arc plasma generator (APG) facilities. 

The APG results have demonstrated that a unique set of apparent kinetic coefficients is deduced for each variety of material tested. The current analysis method, therefore, reduces to little more than an empirical curve-fit of recession rate for a given material as a function of temperature and partial pressure of reacting (or inhibiting) species. No insight regarding the actual ablation mechanisms or important material properties is derived from this approach since no account is taken of the basic material heterogeneity. In addition, the extrapolation of the curve fits derived from the low-pressure and temperature APG environment to the more severe (a factor of 15 in pressure and 1000 to 1500°R in temperature) rocket nozzle environment is uncertain at best.

This program was undertaken to design an experimental approach which will provide materials kinetic data at temperature/pressure conditions of interest without mitigating flowfield/roughness effects. The ultimate objective of the program was to deliver and install a kinetic test cell at AFRPL which could be operated by AFRPL personnel to conduct fast, low-cost generation of kinetic data and materials for heterogeneous studies in-house. The specific objectives were to: a) design and manufacture an experimental apparatus for isolating the kinetic reaction of Hydrogen and G-90 graphite, at temperatures to 6500°R and pressure to 50 atmospheres, b) provide experimental flexibility to accept up to three reactant gases simultaneously, c) develop procedures for heterogeneous material kinetic data reduction, d) deliver and install the experimental kinetics cell at the AFRPL, and e) provide AFRPL with operating and maintenance procedures for the personnel who will be operating the facility on in-house research programs.

Integration of the test cell in the test facility was completed 28 Jul 78. At present, the apparatus is being checkout tested at the AFRPL under the in-house program Carbon/Carbon Processing Variables Investigation, JON 230712KS.

UNCLASSIFIED

SECURITY CLASSIFICATION OF THIS PAGE(When Data Entered)

TABLE OF CONTENTS

<u>Section</u>		<u>Page</u>
1	INTRODUCTION AND SUMMARY	3
2	DESIGN STUDY AND FABRICATION OF A KINETIC TEST CELL	5
	2.1 Flowfield Consideration	7
	2.1.1 Heterogeneous Reactions	7
	2.1.2 Experimental Approach	9
	2.2 Experimental Kinetic Test Cell Design	10
	2.3 Analysis of Kinetics Test Cell Design	19
	2.3.1 Thermal Analysis	20
	2.3.2 Surface Kinetics and Flowfield Size Analysis	22
	2.4 Fabrication	24
	2.4.1 Checkout Runs	26
	2.4.2 Test Facility Layout Recommendation	26
3	HETEROGENEOUS MATERIAL KINETIC DATA REDUCTIONS	28
	3.1 Test Data Acquisition	28
	3.2 Reactions Kinetics	31
	3.3 Test Data Reduction	38
	3.4 Summary	40
4	INSTALLATION OF KINETICS TEST CELL AT AFRPL	42
5	CONCLUSIONS AND RECOMMENDATIONS	43
6	APPENDIX A OPERATING PROCEDURES AND SAFETY	A-47

Accession For	
NTIS GRA&I	<input checked="checked" type="checkbox"/>
DDC TAB	<input type="checkbox"/>
Unannounced	<input type="checkbox"/>
Justification	
By _____	
Distribution/_____	
Availability Codes	
Dist	Availand/or special
A	

LIST OF TABLES

<u>Table Number</u>		<u>Page</u>
1	Experimental Kinetics Test Cell Design Objectives	6
2	Recommended Data Points for Checkout	41

LIST OF FIGURES

<u>Figure Number</u>		<u>Page</u>
1	Tentative Facility Installation Layout	6
2	Solid-Gas Reactions	8
3	DC Resistance Version of Design No. 1	11
4	RF Hollow Cylinder Test Specimen Insert	12
5	Contact Resistance of Electrode Materials	13
6	Resistive Heated Dual Power Kinetics Test Cell	15
7	Inductive Heating Mode of Dual Power Kinetic Test Cell	15
8	Baseline Solid Cylinder Cross Flowfield Concept	16
9	Flowfield Design Adopted for AFRPL Kinetic Test Cell	17
10	Pressure Chamber and DC Heating Supply Adopted for AFRPL Kinetic Test Cell	17
11	Exploded View of Kinetic Test Cell Assembly	18
12	Kinetics Test Specimens	21
13	Estimated Temperature Response to Specimen Size	21
14	Ratio of Diffusion Rate (\dot{m}_D) to Surface Reaction Rate (\dot{m}_r) for Hydrogen. (For $\dot{m}_D/\dot{m}_r > 1$, the Reaction is Kinetically Controlled)	23
15	Rocket Nozzle Material Ablation ATJ Bulk Graphite - Hydrogen Gas	25
16	Cutaway of Electrode/Expansion Assembly	26
17	Schematic of Kinetic Test Cell Assembly	27

Section 1
INTRODUCTION AND SUMMARY

The present interest in carbon composite and bulk polycrystalline graphite materials for solid propellant rocket nozzles has occurred primarily due to the poor thermostructural performance of conventional pyrolytic graphite throat inserts as propellant flame temperature is increased. Circumvention of this problem has necessitated complex, multi-component nozzle configurations which are not only costly to fabricate but inherently less reliable than an integral design. Composite materials, in particular carbon-carbon composites, offer the potential of considerable improvement in manufacturing, reliability and performance attributes compared to pyrolytic graphite. However, their ablation response in the primarily rate-controlled ablation regime of rocket nozzles is poorly understood. At the present time their ablation response is being assessed using the same techniques previously applied to non-porous pyrolytic graphite; e.g., evaluation of the kinetic coefficients from measurements of recession rate in arc plasma generator (APG) facilities.

The APG results have demonstrated that a unique set of apparent kinetic coefficients is deduced for each variety of material tested. The current analysis method, therefore, reduces to little more than an empirical curve-fit of recession rate for a given material as a function of temperature and partial pressure of reacting (or inhibiting) species. No insight regarding the actual ablation mechanisms or important material properties is derived from this approach since no account is taken of the basic material heterogeneity. In addition, the extrapolation of the curve fits derived from the low-pressure and temperature APG environment to the more severe (a factor of 15 in pressure and 1000 to 1500°R in temperature) rocket nozzle environment is uncertain at best.

A program was undertaken to design an experimental approach which will provide materials kinetic data at temperature/

pressure conditions of interest without mitigating flowfield/roughness effects. The ultimate objective of the program was to deliver and install a kinetic test cell at AFRPL which could be operated by AFRPL personnel to conduct fast, low-cost generation of kinetic data and materials for heterogeneous studies in-house. The specific objectives were to a) design and manufacture an experimental apparatus for isolating the kinetic reaction of Hydrogen and G-90 graphite, at temperatures to 6500°R and pressure to 50 atmospheres, b) provide experimental flexibility to accept up to three reactant gases simultaneously, c) develop procedures for heterogeneous material kinetic data reduction, d) deliver and install the experimental kinetics test cell at AFRPL, and e) provide AFRPL with operating and maintenance procedures for the personnel who will be operating the facility on in-house research programs.

The results of these efforts are summarized in order of listing in following sections with conclusions and recommendations inserted as a separate entry.

Section 2

DESIGN STUDY AND FABRICATION OF A KINETIC TEST CELL

The objective of this effort was to design, manufacture, and install a static laboratory kinetic test apparatus with which AFRPL can obtain kinetic data for rocket nozzle materials at temperatures to 6500°R and at reactant pressures up to 50 atmospheres (750 psi). Since AFRPL was to provide the experimental laboratory facility along with the power source for specimen heating, gas supply and transport mechanisms, and test controls and data acquisition techniques, certain constraints were imposed upon the design. Table 1 is a summary of design requirements and equipment type to be provided by AFRPL upon delivery and installation and Figure 1 is a schematic of the AFRPL testing laboratory which served as a model for the design of the kinetic test cell and associated plumbing, power, and diagnostics.

The design constraints essentially reduced to limitation of the available power source (type) and supply. With the power limited to DC resistive heating from a total source of 40 kw, the size of the test specimen and the gaseous flowfield size and configuration became the limiting factor based upon heterogeneous reaction considerations. These dominated design analysis and forced the design of the kinetic test cell to a low velocity gas flow scheme which marginally meets the upper limit design goals (6500°R and 50 atmospheres). However, in anticipation that it may eventually become necessary to modify the power source and the gas reactant pressurization and transport mechanisms, SAI/MSO incorporated materials and configuring (flowfield) options into the final design.

The results of the design study including consideration leading to the design and fabrication follow.

Table 1
Experimental Kinetics Test Cell
Design Objectives

Design Goals;

Specimen Temperatures:	-4000°R-6500°R
Pressure:	-Up to 50 Atmospheres
Reactants:	-Must accept three test gases (H_2 , CO_2 , H_2O) simultaneously
Power Source:	-Limited to 40kw silicon rectifier (DC), 1000 amps
Gas Supply:	-High pressure gas bottles 2200 psia, 200 scfm typical
Adaptability:	-Compatible with existing AFRPL Facility and Instrumentation

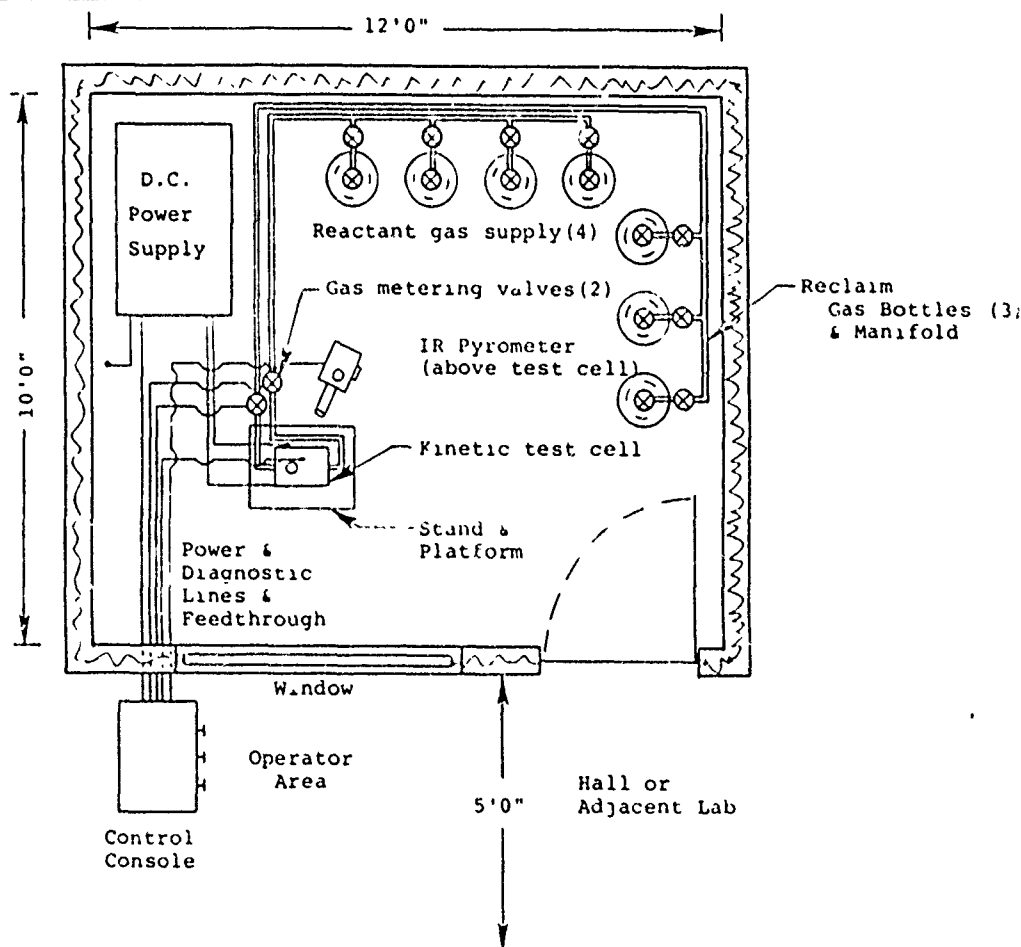


Figure 1. Tentative Facility Installation Layout

2.1 Flowfield Considerations

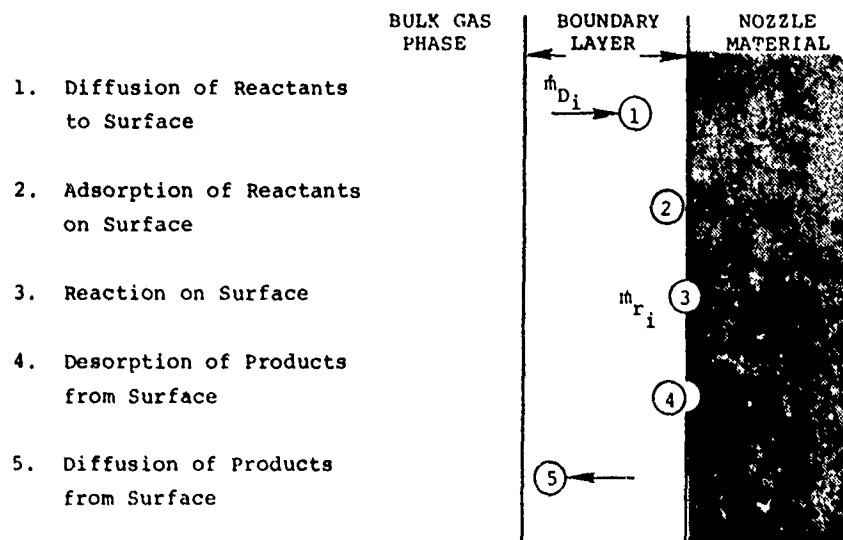
2.1.1 Heterogeneous Reactions. Solid-gas reactions normally involve a series of five steps (see Figure 2). These are:

(1) diffusion of reactants to the solid surface (including the effect of possible gas-phase reactions on the reactant concentration), (2) adsorption of reactants on the surface, (3) reaction on the surface, (4) desorption of products of the reaction and (5) diffusion of products away from the surface. The overall reaction rate will be limited by the slowest of these steps. Thus, the rate may be limited by either (1) surface kinetics (steps 2, 3, and/or 4) or (2) diffusion (steps 1 and/or 5).

If gaseous diffusion is slower than the other steps, convection and mass diffusion within the boundary region completely determine the reaction rate. There are two driving forces for diffusion. First, due to consumption of the reacting species at the solid surface and gaseous recombinations, concentration gradients exist across the boundary region. Product concentration gradients occur simultaneously due to the build-up of product species concentration at the solid surface. A second driving force is due to the thermal gradient across the boundary layer and produces thermal diffusion; i.e., lighter molecules will tend to diffuse to the high-temperature regions and heavy molecules will counterdiffuse to the cooler regions (Reference 1).

The other extreme corresponds to surface kinetics (steps 2, 3 or 4) limiting the overall reaction rate. For this case, diffusional processes will proceed as previously discussed, except at reduced mass fluxes due to the reduction in concentration gradients. When the surface reaction rate is limiting, thermodynamic equilibrium cannot be established at the reaction surface because of the high rate of product mass transfer through the boundary region relative to the rate of surface reactions.

Between these two limiting extremes, the actual reaction rate is often determined both by diffusion in the boundary layer and the nature of the chemical kinetics at the solid surface.



\dot{m}_{D_i} : Diffusion rate of i^{th} reactant

\dot{m}_{r_i} : Reaction rate of i^{th} specie at the surface

- For $\dot{m}_{D_i} \gg \dot{m}_{r_i}$ the reaction is kinetically controlled
- As $\dot{m}_{D_i} / \dot{m}_{r_i} \rightarrow 0$ the ablation rate becomes diffusion limited
- Desire $\dot{m}_{D_i} / \dot{m}_{r_i} > 1$ so that accuracy of the kinetic data is valid.

Figure 2. Solid-Gas Reactions

This is due to the dependence of both phenomena on the concentration of reactant or product species at the gas-solid interface. Without detailed quantitative knowledge of the kinetic rate constant for the surface reaction and the transport properties, it is not possible, a priori, to predict the conditions under which the two limiting extremes exist. This is particularly true in terms of the rocket nozzle environment where, at various times, both limits may exist. In the early stages of firing, when the wall temperature is relatively low and heat transfer rates are high, chemical kinetics may be limiting. As the wall temperature increases, convection and diffusion within the boundary layer

begin to determine the reaction rate.

Section 3 will treat in more detail aspects of the solid-gas reaction model presented above. These will include surface kinetic considerations, diffusion considerations including the pressure dependency of diffusion-controlled reaction as well as temperature dependency of the diffusion controlled reaction, and data derivation methods and techniques for material heterogeneity assessment. The solid-gas reaction model analysis conducted in-depth verified design considerations leading to a flowfield configuration to be discussed in Section 2.2.

2.1.2 Experimental Approach. For any heterogeneous reaction in which a flowing reactive gas stream of constant velocity reacts with a stationary solid, there are temperature and pressure combinations below which the reaction-rate controlling mechanism is represented entirely by the chemical kinetics at the solid surface (adsorption, reaction desorption). If the flow velocity and pressure are kept constant and the temperature is increased, gaseous diffusion becomes the rate determining step of the process. Alternately, if the flow velocity and temperature are kept constant and the pressure is increased, the diffusion becomes rate determining step of the process. Increasing the pressure should decrease the thickness of the boundary region. This decrease, however, is not sufficient to offset the increase in resistance to diffusion through the boundary regions which also results.

This then suggests that temperature and pressure can be used as experimental variables to define the transition regime between kinetic and gaseous diffusion for simple reactive systems. On this basis, a forced flow type flowfield design was selected as the best method of studying the rates of reaction of rocket nozzle materials as a function of temperature and pressure over service environment range. The velocity of flow of reactive gas will be fixed at a constant low value, but sufficiently high to insure a constant free stream concentration. (In part, this modus operandi is dictated by the inability to readily duplicate gas velocity, at least, under the constraints imposed upon the design of the static laboratory test cell).

2.2 Experimental Kinetic Test Cell Design Studies

Experimental objectives and constraints of the AFRPL laboratory test facility imposed upon the design of an experimental kinetic test apparatus were delineated at the beginning of this section and were summarized in Table 1. In addition, at the AFRPL's request the design study initially explored methods of incorporating both DC resistive and radio-frequency (RF) inductive specimen heating modes into a single test article. Two conceptual approaches to a dual power provisioned test apparatus were studied before the AFRPL and SAI/MSO agreed that the objectives of the program could best be met (within the scope of the program) by selecting a design based upon DC resistive heating of the test specimen. In all, four conceptual approaches (designs) to achieving true chemical rates at the temperatures and reactant pressures of interest were studied. A brief description of each follows.

The initial two conceptual approaches evaluated considered designs of dual power provision. Figure 3 presents a schematic of the DC resistive power version of the first concept studied; a design which appeared initially to be very attractive because of the test specimen configuration. The concept (Figure 3) requires test specimens which are hollow cylinders that can (optionally) be configured into the shape of a converging-diverging nozzle. A reactant gas is then expanded through the throat of the test specimen via a pressure drop from the gas inlet to the gas outlet (vent) ports. The hollow cylinder test specimen and the reactant gas is heated resistively (in the DC resistive version) between two graphite electrode assemblies. The graphite electrodes are in turn supplied power through two water cooled copper electrode terminals which also function as structural members of the pressure vessel. The RF inductive power version of this concept requires a coaxial plug in one of the copper electrodes for RF coil feedthrough and replacement of the internal graphite electrode package with a graphite-tungsten susceptibility package (Figure 4).

- | | |
|------------------------------------|---|
| A. Heated Specimen | H. Quartz Pyrometer Window |
| B. Graphite Electrode | I. Teflon Heat Shield |
| C. Graphite Felt Expansion Take-up | J. Mylar Insulator |
| D. Graphite Felt Heat Shield | K. Copper Ends (cooling coil not shown) |
| E. Steel Pressure Cylinder | L. Gas Selector |
| F. Copper Cooling Coil | M. Inert (Argon) |
| G. Insulated Hold Down Bolt | N. Reactive |

O. Mixing Manifold

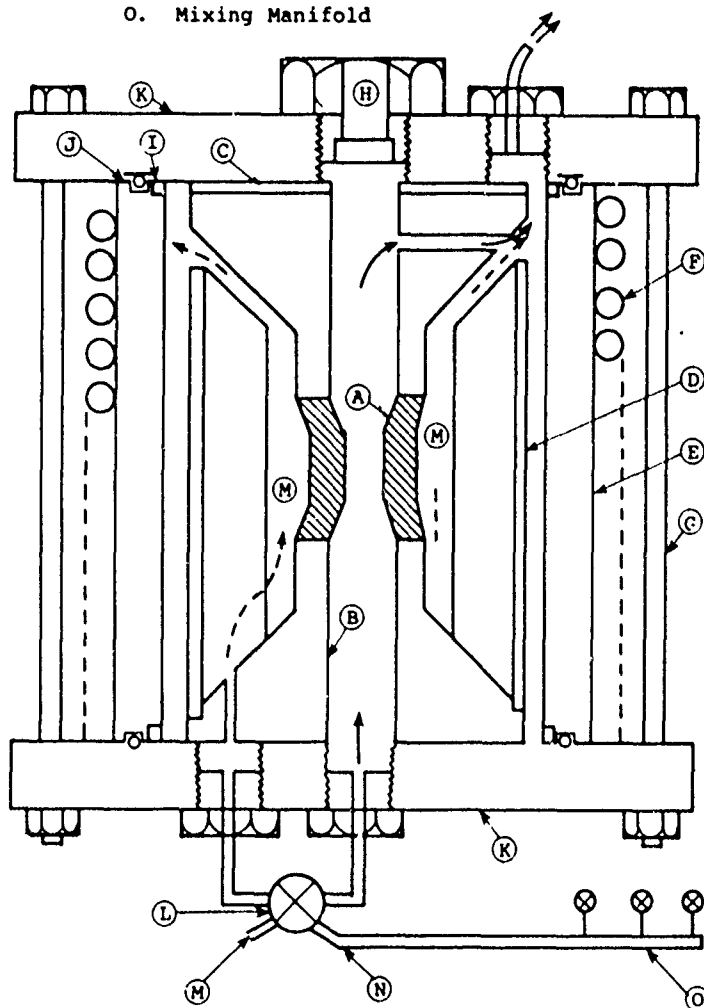


Figure 3. DC Resistance Version of Design No. 1

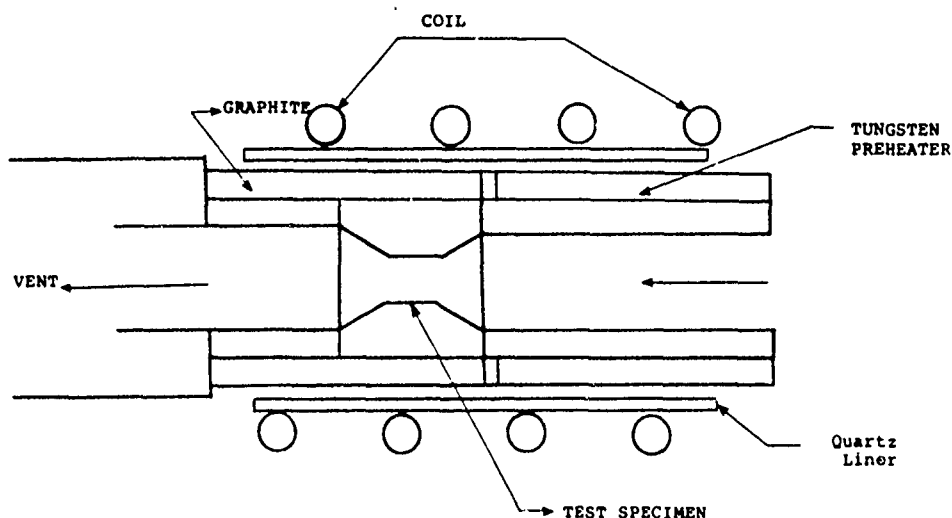


Figure 4. RF Hollow Cylinder Test Specimen Insert

Despite the salient appeal of the simulated nozzle flow conditions to achieving chemical rates in the laboratory, several aspects of the design (Figure 3) were isolated as unacceptable or marginally reliable for in-house research at the AFRPL. Primarily, these had to do with the lack of sufficient power to achieve 6500°R in the test specimen for a hollow cylindrical of sufficient wall thickness. The limitation of 40KW and 25 KW of the AFRPL DC and RF power supplies, respectively, would permit graphite test specimens of less than 0.100 inch wall thickness. Since an ultimate objective of the AFRPL in-house research program is to derive Kinetic data for carbon-carbon materials, this wall thickness is insufficient to achieve ultimate and steady-state temperatures of interest because of the conductivity and anisotropic electrical specific resistivity of carbon-carbons. Secondly, the thin specimen wall thickness could lead to leak paths between the reactant gas on the inside and the inert Argon purge protecting the outside surface of the

test specimen (see Figure 3) due to the high porosity and permeability of the graphites and carbor-carbons of interest to the AFRPL research effort. Finally, structural analysis showed that at very rapid heating rates and/or high chemical reactivity, the thin walled specimens of the design would probably crush under nominal stress loads induced by the experiment.

The feasibility of increasing the power (80KW, 120KW) was investigated for the design (Figure 3) and found not to be efficacious principally because of thermal stress loads which would be induced in the graphite electrode and test specimen assembly because of increased current flow. An increased power availability does not mean a corresponding linear increase in wall thickness and achievable temperatures of the test specimen. Thermal analysis of heating modes in the test specimen configuration conducted for a range and transient conditions of specific resistivities of graphitic materials, as well as consideration of losses due to contact resistance between mating surfaces of different electrode-graphite specimen combinations (Figure 5)

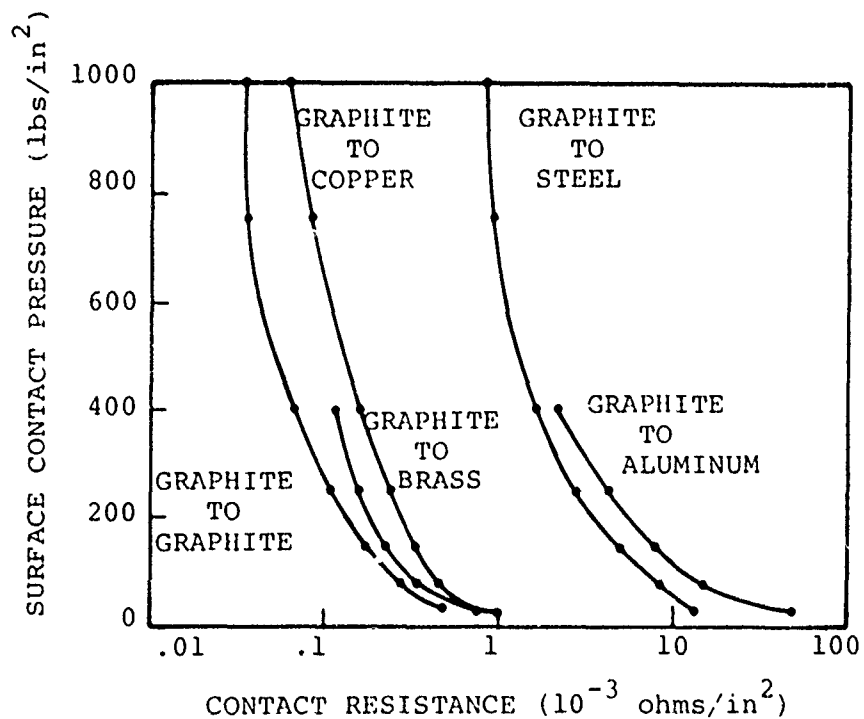


Figure 5. Contact Resistance of Electrode Materials

revealed that steady state conditions would be difficult to achieve and more difficult to reproduce with this conceptual approach. Other concerns, primarily consideration of the AFRPL test facility construction and personnel safety aspects coupled with the uncertainty of experimental reproducibility (specimen temperature and gas flowfield) lead to abandonment of this conceptual approach.

The conceptual approach discussed above was modified in a second attempt to design a dual power test apparatus. Figures 6 and 7 are schematics of the DC resistive and RF inductive power modes of the modified dual power test cell. The concept was eventually abandoned because of the necessity to provide a booster pump to the following reactant and purge gas inlet system in order to achieve the flow velocities required for true chemical rate measurements. A requirement of the AFRPL design criteria for their in-house research program was that the test gases (reactant and purge) be obtained directly from high pressure gas cylinders in order to minimize test facility construction costs and operational safety. The latter was a concern toward the installation of excess electrical equipment in the explosion proof laboratory facility in which the hydrogen reaction experiments are conducted.

A third conceptual approach studied lead to the design which was selected for fabrication (Figure 8). This concept was an attempt to establish a converging reactant gas flowfield prior to impingement upon a cylindrical test specimen. The rationale was to increase the gas velocity by expanding through a nozzle which was intersected by the test specimen and thereby obtain a higher probability of achieving true chemical rates throughout the range of temperature-pressure interest for rocket nozzles. However analysis of the contoured flowfield and the intersecting test specimen showed that turbulent flow conditions would occur throughout the flowfield cavity at pressures of interest and gas velocity actually achievable.

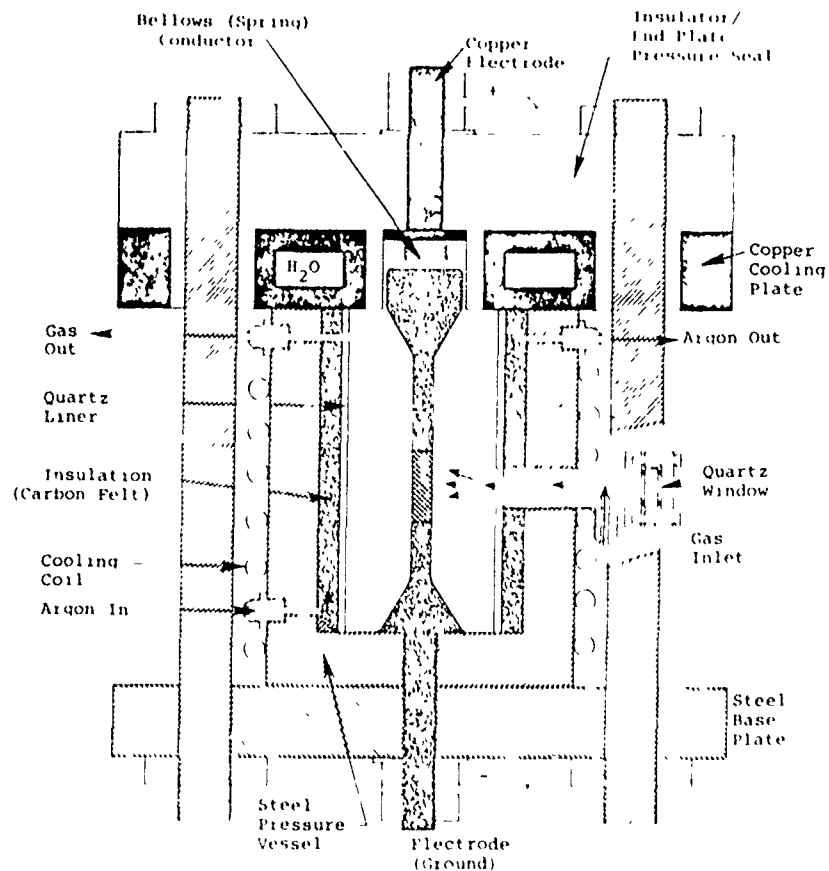


Figure 6. Resistive Heated Dual Power Kinetics Test Cell

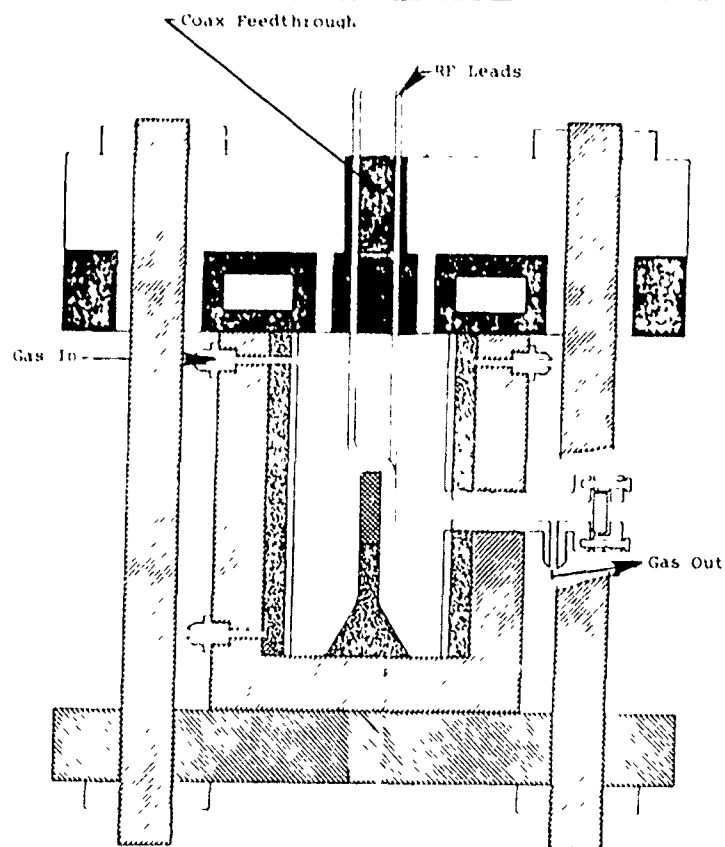


Figure 7. Inductive Heating Mode of Dual Power Kinetic Test Cell

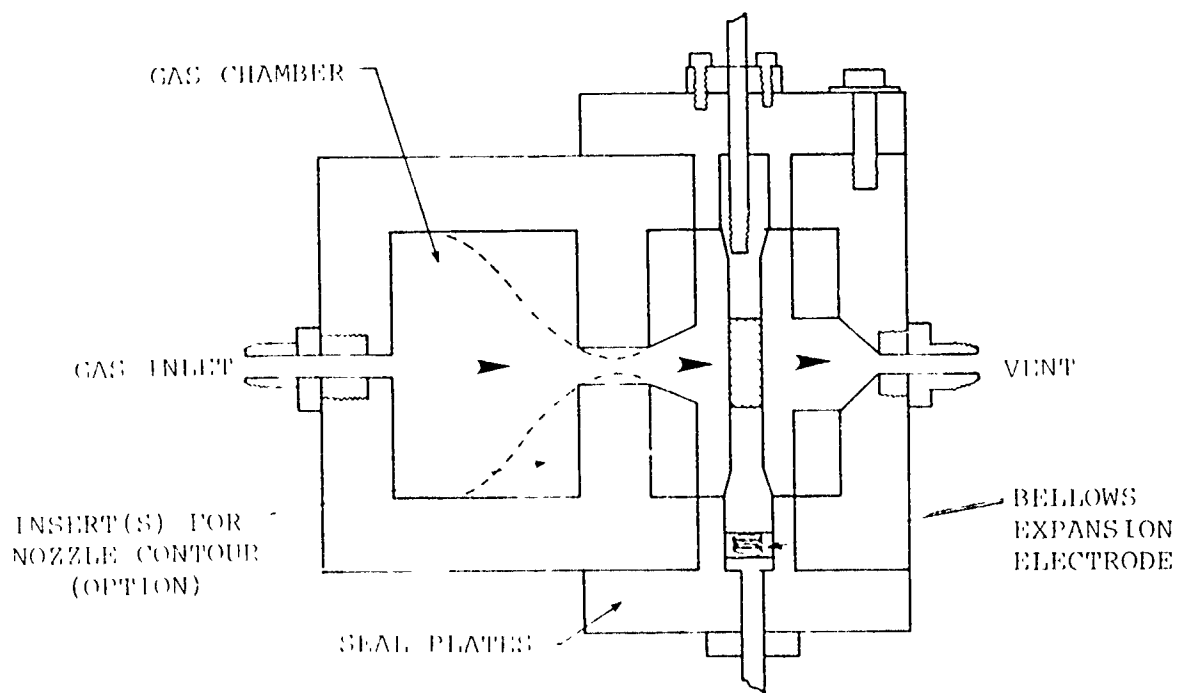
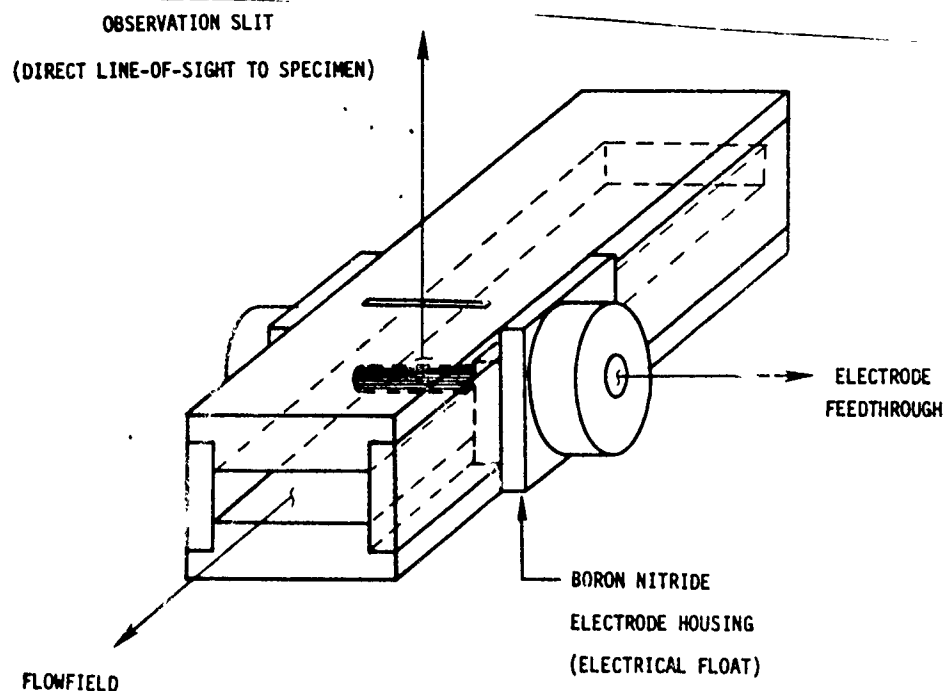


Figure 8. Baseline Solid Cylinder Cross Flowfield Concept

A more optimum flowfield configuration concept for achieving true chemical rates was presented to the APRPL in the second month of effort. The APRPL accepted this approach which led to the conceptualization of the flowfield configuration and pressure chamber shown in Figures 9 and 10, respectively. As shown in Figure 9, the reactant flowfield is a rectangular cross section in which a solid cylindrical test specimen is inserted normal to the flowing reactant gases. The flowfield liner is established in the pressure vessel through a series of interlocking components which can be easily removed for inspection and replacement. The dashed line in Figure 10 shows schematically the open channel for reactant gas flow with the flowfield housing in place in the pressure vessel. Figure 11 is an exploded view of the assembled test cell showing interlocking of the flowfield liner in the pressure vessel.

The greatest difficulty of this design was the method of electrically isolating the electrode feed through by which the test specimens are to be heated resistively while at the



ALL MATERIALS EXCEPT ELECTRICAL INSULATORS ARE ATJ-S

Figure 9. Flowfield Design Adopted for AFRPL Kinetic Test Cell

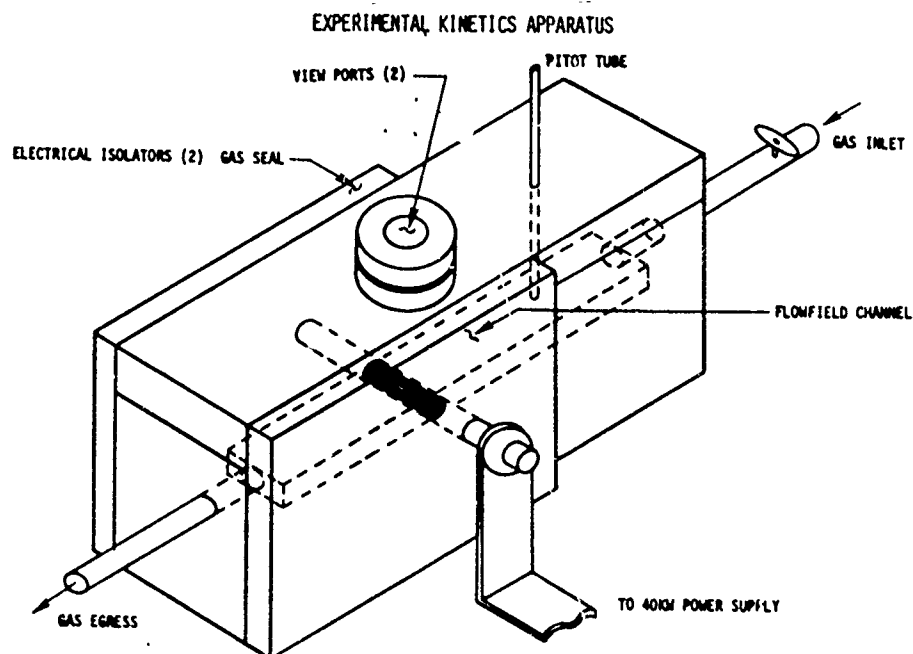


Figure 10. Pressure Chamber and DC Heating Supply Adopted for AFRPL Kinetic Test Cell

THERMAL
BARRIER/
INSULATOR
MYKROY 750

ATJ-S
SPLIT
LINER

VESEL

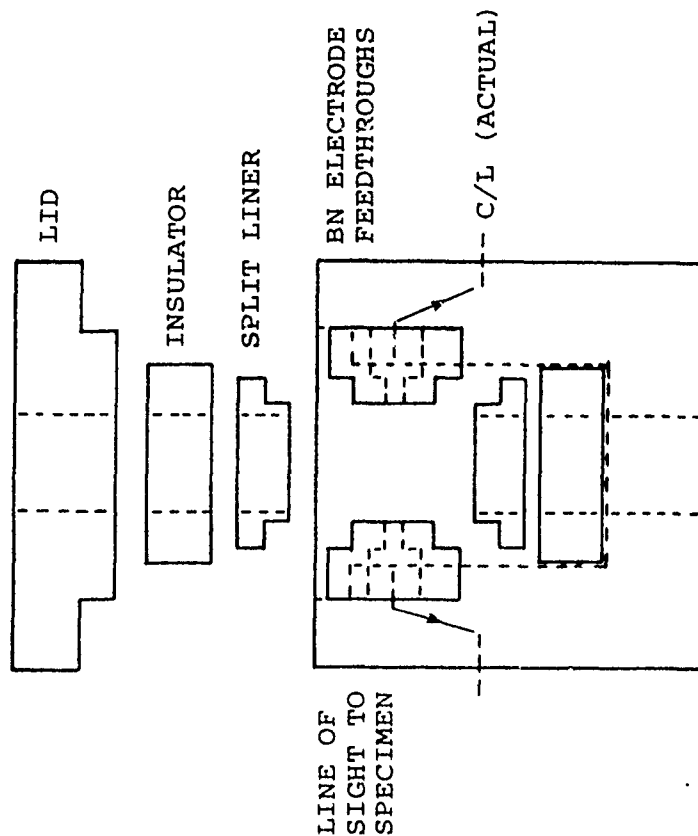
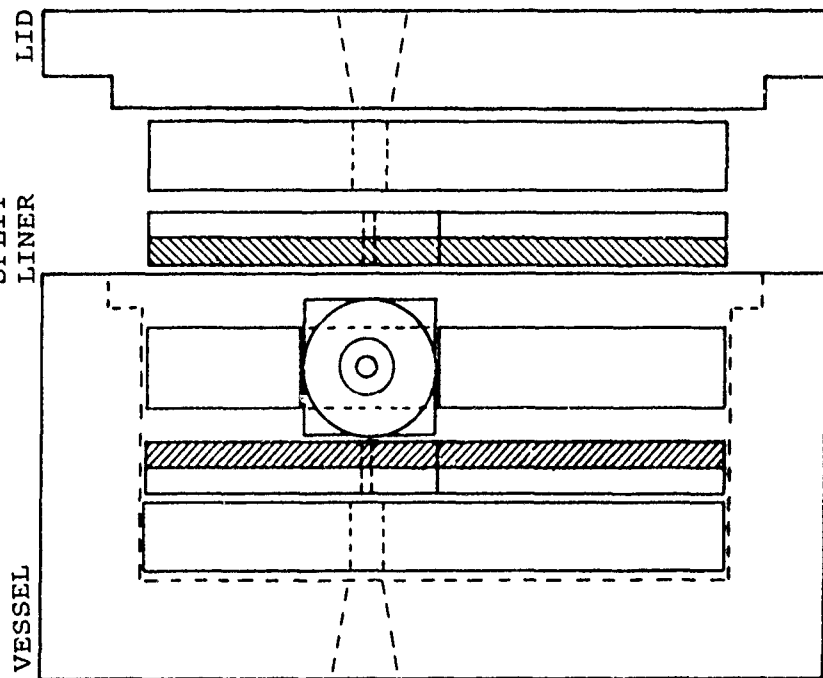


Figure 11. Exploded View of Kinetic Test Cell Assembly

same time maintaining the integrity of the pressure seal. At the same time the electrode must be permitted to move within the electrode feed through and seal in order to compensate for thermal expansion of the test specimens. This facet of the design proved to be the most troublesome eventually requiring a complex seal and feed through configuration to be discussed later.

2.3 Analysis of Kinetics Test Cell Design

Two independent performance analyses of the approved concept described above were conducted following a meeting at AFRPL in the second month of effort. SAI/MSO conducted an analysis of the test specimen thermal response, kinetic reaction consideration, and structural integrity of a baseline configuration of the proposed design. At the request of AFRPL, Acurex Corporation/Aerotherm Division conducted a thermal analysis and surface kinetics study using the same baseline configuration, under their existing AFRPL Contract No. F04611-76-C-0075. The analytical methods and results of the Aerotherm study is presented in Reference 2 and will be discussed in Section 5 which is concerned with conclusions on the efficacy of the SAI/MSO designed AFRPL kinetic test cell. However, it is relevant to point out that oral discussions held with Aerotherm independently at SAI and AFRPL at the conclusion of their study identified potential problems in the design. At the same time, Aerotherm, SAI, and AFRPL were in agreement that useful kinetic data could be derived from the experimental approach, and by modifying the flow parameters, true chemical reactions could be achieved at the design goal of temperatures to 6500 R and reactant pressures to 50 atmospheres.

The Aerotherm study results (Reference 2) which were published after the kinetic test cell pressure vessel was manufactured are less optimistic than either the SAI/MSO analysis or the oral discussion held earlier. Details of these minor disagreements on the performance analysis will be discussed in Section 5 - Conclusions.

2.3.1 Thermal Analysis. The AFRPL Statement of Work placed a constraint upon the power source and level; DC, 1000 amps, 40 kw total. This limitation ultimately drove the final design from all aspects; specimen size, pressure vessel size and options, and gas velocity and flowfield size and configuration. In order to determine specimen size and adequacy of the power supply, a thermal analysis was conducted in which the specimen configuration and size was varied throughout a regimen of gas flow and species reactivity. Further analysis was conducted on the electrical resistivity of graphite types and carbon-carbons with the view that the design should be universal in testing nozzle materials for kinetic reaction data. Ultimately a cylindrical configuration emerged as the only configuration universally acceptable and compatible with the available power.

The test specimen which emerged from these analyses is shown in Figure 12. Assumptions made to obtain a closed-form solution for the temperature distribution in the resistively heated cylindrical test specimen were:

1. Heat losses are due to surface radiation, convection, chemical reaction, and conduction out of its ends.
2. Axial temperature gradients are significantly larger than radial gradients.
3. The ends of the test specimen are held at a constant temperature ($\sim 2000^{\circ}\text{R}$) by external cooling.

Figure 13 shows the results of the analysis relating available power to the test specimen and heat loss to specimen diameter. In order to achieve 6500°R it is necessary to hold the diameter to 0.3-inches because the total heat loss due to conduction, convection, radiation, and chemical reaction approaches 8 kw. The axial length was then established after analysis of the thermal gradients in the test specimen coupled to consideration of the volumetric gas transport requirements, i.e., in order to minimize the amount of gas drawn from the 2000 psi gas bottle supply to be provided by AFRPL. The optimum length

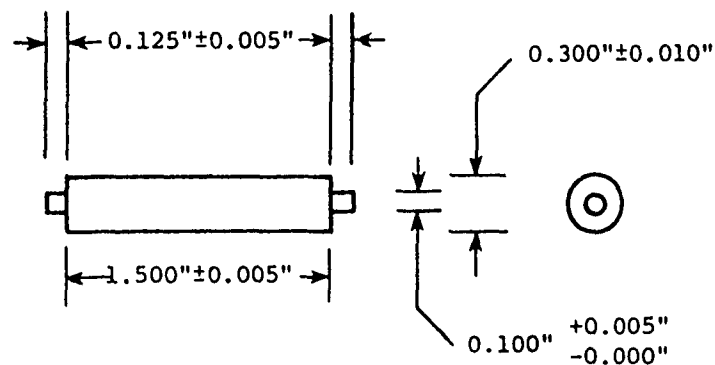


Figure 12. Kinetics Test Specimens

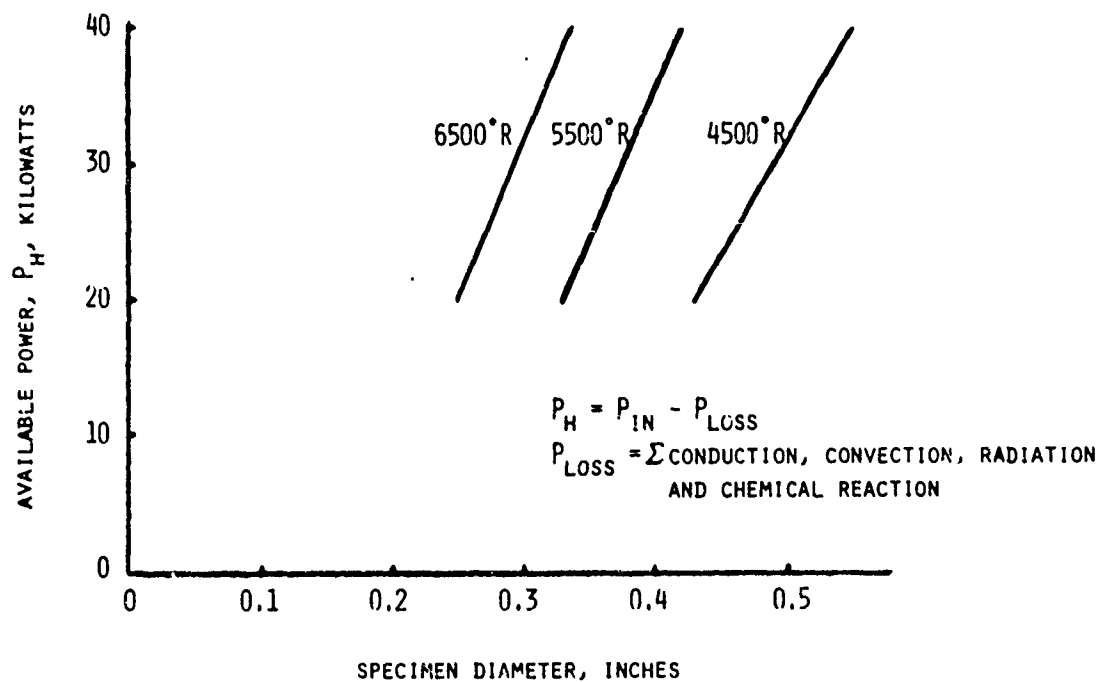


Figure 13. Estimated Temperature Response to Specimen Size

of the test cylinders was determined to be 1.5-inch which will minimize the gas volume consumed in typical test durations. The estimated axial temperature distribution in a 1.5-inch specimen was determined and revealed that the inner 1.0 to 1.2-inch region is at equilibrium where as the outer regions fall rapidly to the temperature of contacted electrodes.

2.3.2 Surface Kinetics and Flowfield Size Analysis. Using the test specimen configuration shown in Figure 12, the chemical reactivity of G-90 and ATJ graphite were modeled for a number of flowfield cross sections (channels) and gas velocities (for Hydrogen only since it represents a worst case approach from a temperature standpoint). Figure 14 presents the results of those analyses for extremes of design options: 1) flowfield channel cross sections of 0.8-in² and 8-in², and 2) forced gas flow at 100 SCFM and 400 SCFM. The curves in Figure 14 are the ratio of $\dot{m}_D/\dot{m}_r/H_2$ where

\dot{m}_D = the diffusion rate of Hydrogen to the surface

\dot{m}_r = reaction rate of Hydrogen at the surface at the Hydrogen partial pressure on the ordinate.

The curves generated in Figure 14 were based upon a calculated heat transfer coefficient (N_C) of 4.33×10^{-2} LBM/FT²-sec derived from the equation for a solid cylinder in a cross flow cavity

$$N_C = 1.368 \, v_{os} \rho_{os} u_{os} / D \text{ where}$$

ρ_{os} = density of the flowing gas

v_{os} = velocity

u_{os} = viscosity

D = diameter of the test specimen

For $\dot{m}_D \gg \dot{m}_r$, the reaction is kinetically controlled and as $\dot{m}_D/\dot{m}_r \rightarrow 0$ the ablation rate becomes diffusion limited (see Section 2.1 for discussion). The theoretical criterion in determining the diffusion controlled limit is $\dot{m}_D/\dot{m}_r = 1.0$. Therefore it is desirable to limit \dot{m}_D/\dot{m}_r to values greater than unity so that the accuracy of the kinetic data derived is good. Therefore it was necessary based upon the results shown in

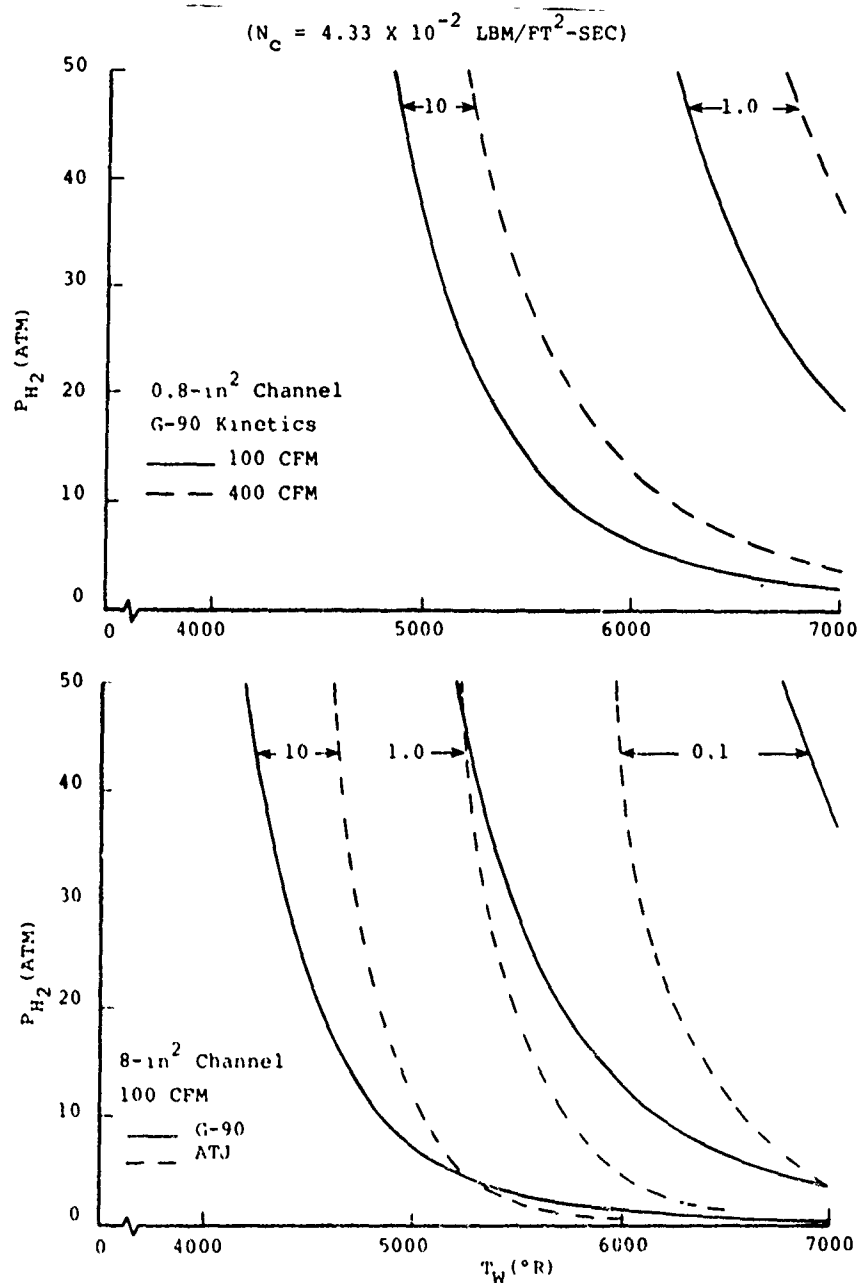


Figure 14. Ratio of Diffusion Rate (\dot{m}_D) to Surface Reaction Rate (\dot{m}_r) for Hydrogen. (For $\dot{m}_D/\dot{m}_r > 1$, the Reaction is Kinetically Controlled)

Figure 14 to limit the flowfield channel to a cross section of approximately 0.8-inch (0.75-inch in final design) and establish flow velocities to exceed 100 SCFM in order to achieve the design goal of 6500°R and 50 atmospheres. An ablation rate analysis was conducted to determine test duration times (Figure 15) for the temperatures of interest.

2.4 Fabrication

Figures 9, 10, and 11 presented schematic views of the baseline design which emerged as a fabricated article in this study. The body of the pressure vessel and the lid are constructed of 304 stainless steel from billets forged for SAI/MSO by Jorgensen Steel, Bethlehem, PA. The wall thickness is 1.25-inches which based upon direct stress analysis for a thick walled pressure vessel provides a factor of safety of 66 at 750 psi. Two end plates of glass cloth laminate (1.25-inch thick) provide electrode access to the test specimen and seal the internal pressure to 750 psi. These end plates provide the lowest factor of safety (10.2) in the vessel construction as based upon calculations of maximum displacement and stress using classical theory of plates and shells analysis methods (Reference 3). The nominal dimensions of the experimental test cell are 6-inch x 6-inch x 12-inch.

The fabrication of all components with the exception of two quartz windows were subcontracted to Algo Tool and Die, Santa Ana, California. The windows were fabricated by Pennfold Optical Company, Santa Ana, California according to SAI/MSO specifications. Materials were selected by SAI/MSO and provide to Algo along with engineering drawings and specifications.

All components of the flowfield liner, electrode housing and seal plates, and pressure gaskets were hand machined to fit in the interlocking pattern shown in Figure 9 and 11. The electrode assembly and tensioning mechanism shown in Figure 16 were developed through rework following initial checkout runs.

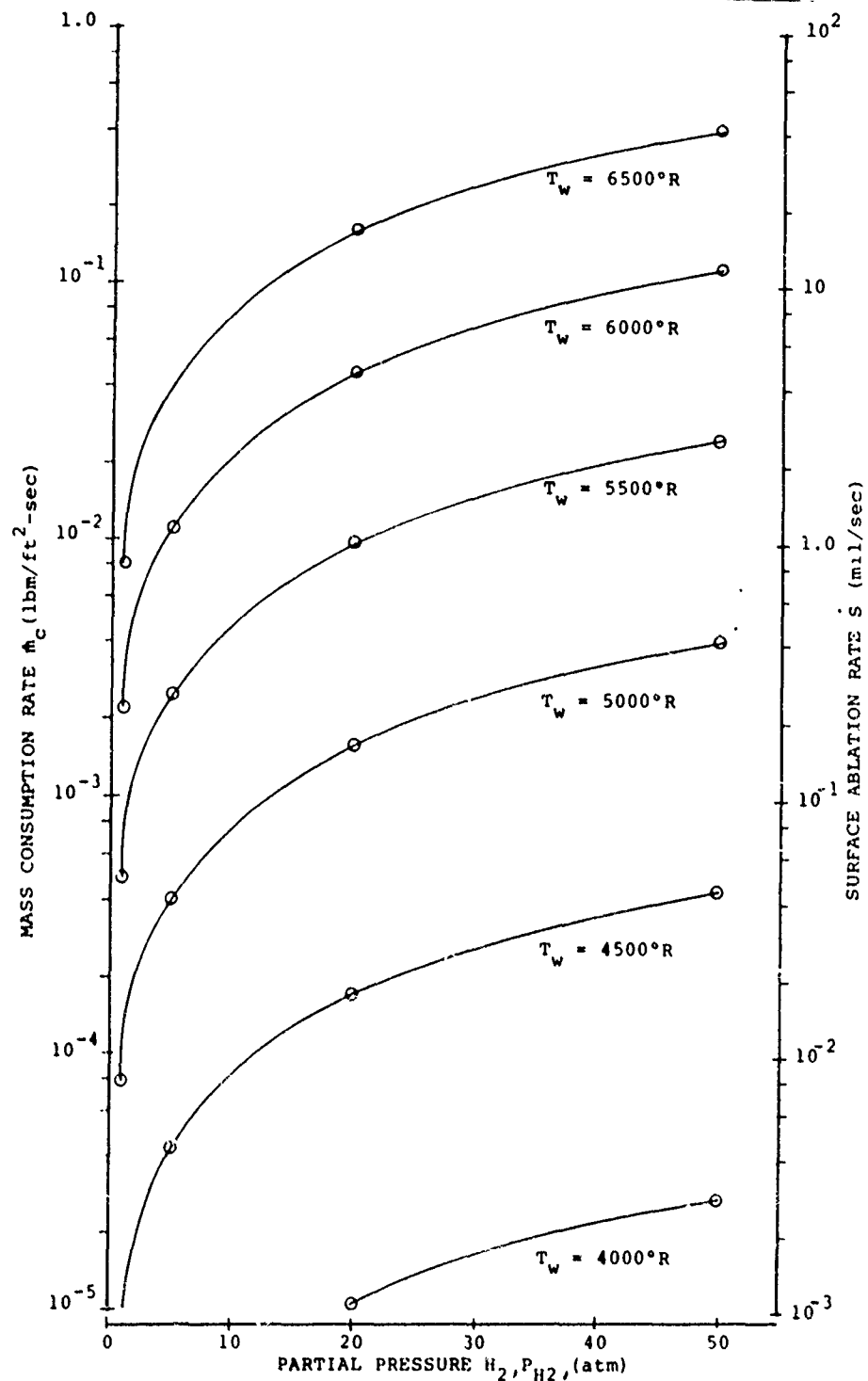


Figure 15. Rocket Nozzle Material Ablation ATJ Bulk Graphite - Hydrogen Gas

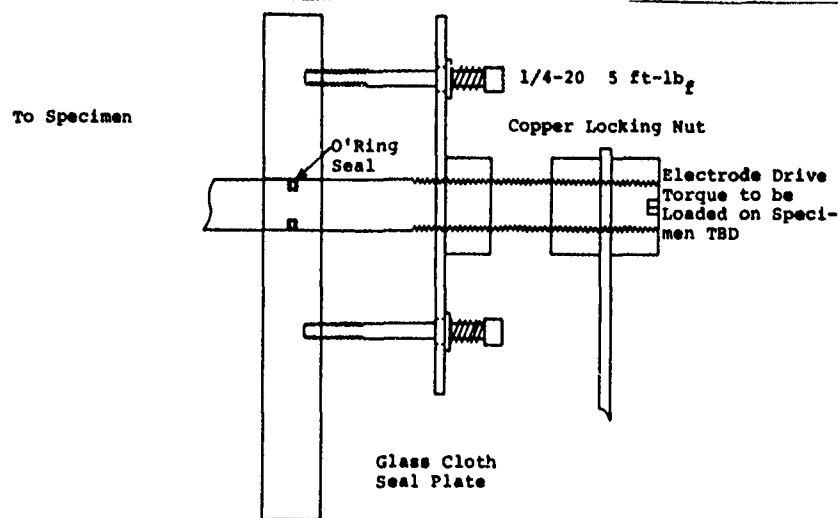
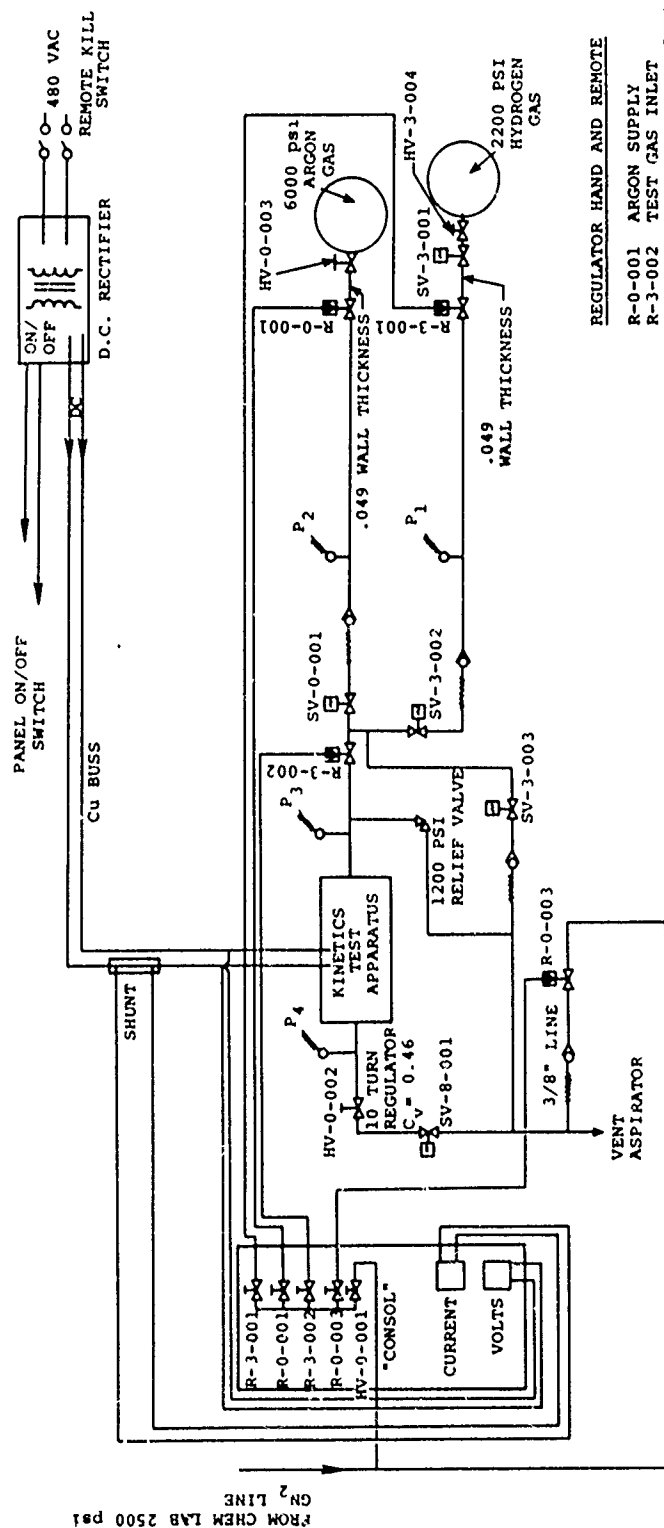


Figure 16. Cutaway of Electrode/Expansion Assembly

2.4.1 Checkout Runs - Prior to delivery at the AFRPL, the assembled kinetic test cell was temporarily installed at SAI using heating and gas flow modes comparable to those being built at the AFRPL test facility. Although limited to 15 kw by the SAI power supply, and unable to flow at design rates, the initial checkout confirmed that the pressure goal of 50 atmospheres was achievable up to temperatures of 5500°R (limit of SAI power) with G-90 specimens. Static pressure tests repeated several times showed no measurable gas loss over 24 hours at 750 psi and ambient temperatures. Time durations of up to five minutes of continuous heating at 5000°R showed that the window ports would not heat appreciably due to the novel thermal barriers of the vessel (Figure 11). These same continuous heating runs also demonstrated the integrity of the high pressure seals designed for this application.

2.4.2 Test Facility Layout Recommended to the AFRPL

Following the checkout runs, technical exchanges between SAI/MSO and the AFRPL operating personnel responsible for installation of the test apparatus were held to ensure the integration of the kinetic test cell into the AFRPL facility. A layout diagram of the recommended operational experimental facility was presented to the AFRPL. Figure 17 is a schematic of the operational test facility that emerged from this effort.



REGULATOR HAND AND REMOTE

- R-0-001 ARGON SUPPLY
- R-3-002 TEST GAS INLET
- R-0-003 ASPIRATOR G N₂ SUPPLY
- R-3-001 G H₂ SUPPLY

SOLENOID VALVES

- SV-0-001 ARGON BOTTLE SUPPLY N.O.
- SV-3-002 REACTANT TEST GAS N.C.
- SV-3-003 REACTANT BY PASS N.C.
- SV-3-001 G H₂ BOTTLE SHUT OFF N.C.
- SV-8-001 TEST GAS OUT N.O.

HAND VALVES

- HV-0-001 2500 psi GN₂ SUPPLY TO PANEL
- HV-0-002 10 TURN REGULATOR
- HV-0-003 6000 psi REDUCING REGULATOR
- HV-3-004 2200 psi SOURCE REGULATOR

Figure 17. Schematic of Kinetic Test Cell Assembly

Section 3

HETEROGENEOUS MATERIAL KINETIC DATA REDUCTION

In this section an outline of the procedure for deriving kinetic coefficients from the test data to be generated at AFRPL is presented. Direct application of the techniques described have not been implemented since data for the G-90 material has yet to be generated. For this reason, the techniques may require some modification as test data is generated and experience with the experimental apparatus is developed.

The basis for the SAI approach to generate kinetic coefficients from the test data to be obtained using the AFRPL Kinetics Test Cell is an analytical model for the ablation of a porous solid. Through this model the effects of material heterogeneity are explicitly included; it is anticipated that the future acquisition of test data on a wide range of materials having well-characterized properties, definitive relationships between kinetic coefficients and measurable material properties such as internal open surface area, permeability, porosity (see Reference 1), and anisotropy (see Reference 2) will be established. Because the present effort is limited to a single material (G-90) and test gas (H_2) these relationships cannot be derived from the test data and will not be discussed further.

3.1 Test Data Acquisition

As noted above, under the current study the ablation test data to be obtained from the Kinetics Test Cell is limited to a single material and a single pure test gas, hydrogen. Data to be obtained for each test point include the following:

- a) average specimen surface temperature, T_w (K)
- b) average recession rate, \dot{s} (cm/s)
- c) average specimen surface pressure, P_w (atm)
- d) average no blowing heating transfer coefficient,
 $\rho_e u_e C_{H_2O}$ ($g/cm^2 \cdot s$)

The measurement of each of these quantities is discussed in the following paragraphs.

Test specimen surface temperature is measured throughout the test duration using a pyrometer focused on the top, center of the test specimen as far forward (toward the stagnation point) as is practical without the spot falling off the specimen. An observation slit has been provided in the flow field channel for this purpose (see Figure 9). Average surface temperature is determined from the reduced pyrometer data from either the temperature-time trace directly or in combination with the specimen recession-time history if laser measurement of instantaneous recession is obtained.

The average specimen recession rate can be determined in two ways. The first and simplest approach is to use specimen pre- and post-test dimensional changes and the average test time. In this case, the post-test specimen is chucked in a lathe or similar rotatable holding fixture using the holding pins at each end of the specimen (see Figure 12) to establish the centerline. A dial gauge is then used to measure the radius of the specimen as a function of angular position from the stagnation line. These measurements may be repeated at several axial stations along the specimen but near the axial center of the specimen. Using this "map" of measurements, the pre-test radius, and the test time the average recession rate can be calculated from the equation

$$\dot{s} = \frac{1}{t_t n} \sum_{i=1}^n (R_o - R_f)_i \quad (1)$$

where

t_t = test time(s)

R_o = specimen initial radius (cm)

R_f = specimen final radius (cm)

and n is the number of measurements made. An alternate approach may be utilized if a laser system is used to measure instantaneous surface position again employing the observation slit provided.

In this case, the reduced laser system data yields the stagnation region radial location as a function of time throughout the test duration. This data can be plotted on linear graph paper and the best-fit slope (\dot{s}) obtained for the central portion of the test data. The laser method is obviously more advantageous than the pre- and post-test measurement technique since start-up and shut-down transients (and other anomalies which may appear occasionally) can be excluded from the data. However, it is anticipated that because of the basic test procedure (e.g., pre-heating the sample resistively eliminates the usual transient associated with specimen heat-up and purging the kinetics cell with non-reactive argon at the end of the test eliminates further ablation during cool-down), transients will be relatively small and the first method will provide acceptable data accuracy.

The specimen surface pressure (P_w) is very nearly identical to the pressure measured by the line inlet pressure gauge (P_3 in Figure 17) since the test cell flow Mach numbers are much less than one. Maximum operating Mach number occurs at the condition of maximum test cell flow rate of 300 cfm and minimum pressure of 1 atm and is approximately 0.1. Maximum pressure drop from stagnation conditions is 0.7 percent for and therefore the error in P_3 relative to the average specimen wall pressure is less than one percent.

Measurement of the heat transfer coefficient always presents a difficult problem in experimental ablation testing. Because of the unique attributes of the Kinetics Test Cell, SAI suggests a combined experimental and analytical technique to obtain $\rho_e u_e C_{H_2O}$. The basic technique involves measuring the cool-down rate of the specimen from some initial temperature with the non-reactive argon gas flowing using the pyrometer to obtain the surface temperature-time history. Two variants are possible. In the first method special calibration runs of the apparatus are made at selected pressures and flow rates. The specimen is brought to a fixed temperature using the DC rectifier with argon gas flowing. After the specimen has equilibrated the power to

the DC rectifier is turned off and the specimen is allowed to cool down with the argon gas continuing to flow. The resulting temperature-time history obtained from the pyrometer can then be analyzed using a 2-D transient heat conduction code in an iterative manner to obtain the heat transfer coefficient which best matches the cool-down history. The thermal properties of the specimen (conductivity, heat capacity, and emissivity) are of course required for this analysis. The heat transfer coefficient at other pressures and flow rates are obtained from interpolation of the data from the selected calibration points. In the second variant, the same basic approach is utilized except that for each ablation test data point, the cool-down history is monitored by the pyrometer and the heat transfer coefficient obtained directly for that point. Experience to be gained with the apparatus will dictate which of these two approaches is best suited to the efficient acquisition of accurate data.

3.2 Reaction Kinetics

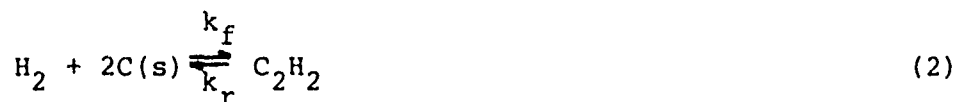
In this section a description of the reaction of a porous, heterogeneous carbon surface with a single component gas is given. In principle, the analysis applies to multi-component gases; however, this situation is beyond the scope of the present effort and will not be discussed.

The analytical model proposed by SAI for the reduction of test data from the Kinetics Test Cell considers the following three regimes. At low temperatures where the reactivity of the solid carbon is low, a molecule of gaseous reactant may enter the porous solid and has a high probability of diffusing into the material before finally reacting with the pore surface. In this region the concentration of gaseous reactant is essentially uniform through the porous solid and equal to that at the solid surface. The overall reaction rate is comprised mainly of the reactions taking place within the material since the exposed reaction area internally is several orders of magnitude greater than the external surface area.

At higher temperatures where the solid reactivity is greater, the probability of the gaseous reactant molecule penetrating deeply within the material before reacting is small. Both chemical reaction rate and pore diffusion exert an influence on the overall reaction rate in this regime. However, as temperature is further increased the surface reaction begins to dominate the ablation rate.

In general, as even higher temperatures are considered the reaction rate of the solid material will become sufficiently large that the kinetics of the reaction will no longer control the overall reaction rate. This regime is the so-called diffusion-limited regime. In actuality this regime is simply the chemical equilibrium regime wherein the wall partial pressures of the reactant and the reaction product are in chemical equilibrium with the solid material. The more familiar diffusion-limited result occurs only when the equilibrium constant for the reaction is such that complete reaction of all the reactant occurs and the wall partial pressure of the reactant approaches zero. In the equilibrium regime the overall reaction rate is controlled by the equilibrium constant for the reaction and the mass transfer coefficient of the boundary layer.

Consider now the specific reaction to be characterized



The forward reaction rate coefficient, k_f , is assumed to be given by an Arrhenius form

$$k_f = k_o T^a \exp(-E/RT) \quad (3)$$

and the corresponding intrinsic forward reaction rate is

$$\dot{m}_f = k_f [(P_{\text{H}_2})_w]^n \quad (4)$$

where

- k_f = forward reaction rate ($\text{g/cm}^2\text{-s-atm}^n$)
- k_o = kinetic coefficient ($\text{g/cm}^2\text{-s-K}^a\text{-atm}^n$)
- a = temperature exponent
- E = activation energy (cal/gmole)
- R = universal gas constant ($1.986 \text{ cal/gmole-K}$)
- $(P_{H_2})_w$ = hydrogen partial pressure at wall (atm)
- n = reaction order
- \dot{m} = reaction rate of carbon ($\text{g/cm}^2\text{-s}$)

For an irreversible [$k_r \rightarrow 0$ in Eq. (2)], equimolar reaction, the overall reaction rate of a porous solid is given as (see Reference 3)

$$R_s = \left(\frac{2}{n+1}\right) k' S_v D_e^{1/2} (C_{H_2w})^{\frac{n+1}{2}} + k' f (C_{H_2w})^n \quad (5)$$

where

- R_s = rate of reaction per unit time per unit geometric external surface area ($\text{gmole of reactant/cm}^2\text{-s}$)
- S_v = internal surface area per unit volume (cm^{-1})
- D_e = effective gas diffusivity (cm^2/s)
- C = gas molar concentration (gmole/cm^3)
- f = ratio of true external surface area to geometric (projected) surface area
- k' = forward reaction rate ($\text{gmole}^{1-n}\text{-cm}^{3n-2}/\text{s}$)

Eq. (5) is generally derived in terms of concentration of the reacting gas species since for pore diffusion, concentration rather than partial pressure is the more natural dimensional quantity. However, Eq. (5) can be cast in the more conventional (at least to rocket motor ablation analysts) form of Eq. (4) by equating the intrinsic forward reaction rates and noting that

$$C_{H_2w} = P_{H_2w}/RT_w \quad (6)$$

where R is again the universal gas constant (82.06 cm³-atm/gmole-k). Eq. (5) then becomes

$$\dot{m} = k_f (P_{H_2w})^n + \left[\left(\frac{2}{n+1} \right) k_f \phi M_{H_2} S_v D_e / RT_w \right]^{1/2} (P_{H_2w})^{\frac{n+1}{2}} \quad (7)$$

where

M_{H_2} = molecular weight of H₂ (2.016 g/gmole)

ϕ = grams of C(s) reacted per gram of H₂ (11.92)

In Eq. (7) the roughness factor, f , has been set equal to one in conformity with standard practice due to the difficulty of defining the true exposed external surface of a porous solid.

Eq. (7) is the basic equation expressing the overall mass loss rate of a porous carbon surface in terms of the reactant partial pressure at the wall, the intrinsic kinetic reaction rate, k_f , and the material related parameters, S_v and D_e . S_v is dependent primarily on the microstructure of the porous carbon and may be obtained from the commonly measured value of S_α , the open internal surface area per unit mass, via the equation

$$S_v = \rho_o S_\alpha \quad (8)$$

where ρ_o is the bulk density of the material. The effective gas diffusivity, D_e , depends on both the flow regime and material microstructure. For the low-density Knudsen flow regime

$$D_e = \frac{4}{3} \left(\frac{8RT_w}{\pi M_{H_2}} \right)^{1/2} B \quad (9)$$

where B is the molecular permeability coefficient of the material expressed in centimeters and commonly measured (see Reference 1). For the small pore sizes typical of graphitic carbon material, the Knudsen flow regime extends to pressures on the order of several atmospheres. However, at sufficiently high pressures the molecular diffusion limit will be approached. In this case one has

approximately

$$D_e = (\epsilon/\tau) D_{12} \quad (10)$$

where

ϵ = porosity of the solid material

τ = tortuosity factor, ratio of actual path length to geometric path length

D_{12} = molecular diffusivity for gas pair 12 (cm^2/s)

For binary gas mixtures at low pressures (e.g., below 10 atm) and non-polar gases D_{12} can be estimated from the Chapman-Enskog Kinetic theory

$$D_{12} = 0.0018583 \frac{[T^3(M_1^{-1} + M_2^{-1})]^{1/2}}{p\sigma_{12}\Omega_{12}}$$

where D_{12} is in cm^2/s , T is in degrees K, p is in atmospheres, σ_{12} is in Å and Ω_{12} is the collision integral; Ω - a tabulated function of $T/(\epsilon/k) - \sigma$ and ϵ are given for a number of pure gases in Reference 4; and

$$\sigma_{12} = \frac{1}{2} (\sigma_1 + \sigma_2) \quad (12)$$

$$\epsilon_{12} = \sqrt{\epsilon_1 \epsilon_2} \quad (13)$$

The effective diffusion coefficient, D_e , may be in either the Knudsen flow regime or the molecular diffusion regime. For the former

$$D_e \propto B T_w^{1/2} \quad (14)$$

while for the latter

$$D_e \propto (\epsilon/\tau) [T_w^{3/2}/\Omega_{12}(T_w)]/P_w \quad (15)$$

where B and (ϵ/τ) are constant material parameters. At the present time, it is expected that Knudsen flow will predominate; however, this assumption must be verified by the experimental data to be obtained in the Kinetics Test Cell tests.

In summary, Eq. (7) provides the theoretical form assumed to govern the kinetic mass loss rate of a porous material. The kinetic rate coefficient k_f is assumed to be of the form given in Eq. (3). It remains to develop the boundary layer diffusion equations which will allow determination of the reactant partial pressure at the wall.

For the present reaction system (Eq. 2) assuming equal diffusion coefficients of the gas phase species, the boundary layer diffusion equations reduce to the following (see Reference 5)

$$\tilde{K}_{Cw} = \frac{B'}{1 + B'} \quad (16)$$

$$K_{Hw} = \frac{\tilde{K}_{He}}{1 + B'} \quad (17)$$

where

$B' =$ normalized mass transfer rate, $\dot{m}/\rho_e u_e C_M$

$C_M =$ mass transfer parameters, $C_M = C_H Le^{2/3}$

$C_H =$ Blowing value of the Stanton number

$L_e =$ Lewis number

$\tilde{K}_i =$ mass fraction of i^{th} element

C_H is related to the non-blowing Stanton number, C_{Ho} , via the usual correlation equation

$$\frac{C_H}{C_{Ho}} = \frac{2\lambda\dot{m}/\rho_e u_e C_{Ho}}{\exp(2\lambda\dot{m}/\rho_e u_e C_{Ho}) - 1} \quad (18)$$

where λ equals 0.4 for turbulent boundary layers.

Eqs. (15) and (17) define the mass transfer rate, B' , if chemical equilibrium is assumed. For the case of no sublimation, the solution is simply

$$B'_{eq} = \phi \tilde{K}_{He} \left(\frac{K_p}{1 + K_p} \right) \quad (19)$$

where K_p is the equilibrium constant for the reaction; i.e.,

$$K_p = \frac{P_{C_2H_2}}{P_{H_2}} \quad (20)$$

An equation similar to Eq. (19) could be written allowing carbon sublimation involving the vapor pressures of the various carbon gas species ($C_1 - C_i$). Equation (19) may also be written as

$$B'_{eq} = \frac{\phi [\tilde{K}_{He} - K_{H_2w}]}{1 + \phi K_{H_2w}} \quad (21)$$

where K_{H_2w} is the mass fraction of the reactant gas (H_2) at the wall. Eq. (20) makes clear the earlier comment that the diffusion-limited rate is not reached until complete reaction of the H_2 reduces K_{H_2w} to zero.

Alternately, when the kinetic reaction rate is slow and chemical equilibrium is not attained Eqs. (16) and (17) may be solved for the wall mass fraction of H_2 in terms of B' ; e.g.,

$$K_{H_2w} = \frac{\tilde{K}_{He} - B'/\phi}{1 + B'} \quad (22)$$

For \tilde{K}_{He} identically equal to one, i.e., the test condition for the initial test series, one has

$$\frac{P_{H_2w}}{P_w} = \frac{(MC_{2H_2}/M_{H_2}) K_{H_2w}}{1 + \phi K_{H_2w}} \quad (23)$$

Hence, the boundary layer diffusion equations define the wall pressure of the reactant via Eqs. (22) and (23) in terms of the normalized mass transfer rate, B' .

In Section 3.3, the theoretical results derived are applied to the reduction of test data from the Kinetics Test Cell.

3.3 Test Data Reduction

The basic test data measured for each data point obtained in the Kinetics Test Cell are \dot{s} , $\rho_e u_e C_{H_2O}$, T_w , and P_w as discussed in Section 3.1. The initial data reduction steps consist of obtaining the following quantities:

- a) \dot{m} from \dot{s} and ρ_O from the equation

$$\dot{m} = \dot{s} \rho_O \quad (24)$$

- b) $\rho_e u_e C_H$ from \dot{m} and $\rho_e u_e C_{H_2O}$ via Eq. (18)

- c) $\rho_e u_e C_m$ from $\rho_e u_e C_H$ using the equation

$$C_m = C_H (Le)^{2/3} \quad (25)$$

- d) B' from $\rho_e u_e C_m$ and \dot{m} from the definition of B'

$$B' = \dot{m} / \rho_e u_e C_m \quad (26)$$

- d) P_{H_2w} from Eqs. (22) and (23)

An alternate approach to calculate P_{H_2w} is to exercise the GASKET code (Reference 6) for an open system with B' specified. This code has the advantage of a capability to treat non-equal diffusion coefficients.

Given the initial reduced data described above (\dot{m} , P_{H_2w} , T_2 , P_w) for each data point obtained, it is desired to derive the kinetic coefficients (k_O , a , E , n) for the reaction given by Eq. (2) and the pertinent material properties (S_v and B).

Assuming Eq. (7) describes the overall reaction of H_2 with the porous carbon test material and that Knudsen flow is obtained in the pores, the form of Eq. (7) is

$$\frac{\dot{m}}{(P_{H2w})^{\frac{n+1}{2}}} = A(T_w) + k_f(T_w)(P_{H2w})^{\frac{n-1}{2}} \quad (27)$$

Eq. (27) suggests that an initial test series at varying wall pressures but constant wall temperature could be run to determine the reaction order, n . That is if a series of data points at constant wall temperature are plotted on linear graph paper with the ordinate equal to $\dot{m}(P_{H2w})^{-(n+1)/2}$ and the abscissa equal to $(P_{H2w})^{(n-1)/2}$ for selected values of n , the reaction order is determined by that value of n which yields a straight line. For n not equal to one the best-fit line intercept at P_{H2w} equal zero is A while the slope is k_f . If n equals one then the apparent slope will be zero and the intercept is $(A + k_f)$.

For $n \neq 1$ this procedure repeated at a series of temperatures defines n , k_f , and A as functions of T_w . Since the reaction order is assumed to be a unique constant independent of temperature, the values of n obtained at each temperature should be the same. Due to data scatter the actual values obtained may be slightly different, in which case they should be averaged to obtain a unique value of reaction order, and k_f and A recalculated at each temperature using that value.

At this point (assuming $n \neq 1$) one has deduced values for n , $k_f(T_w)$, and $A(T_w)$. Reference to Eqs. (7), (9), and (27) shows that

$$A^2 = \frac{2}{n+1} k_f \phi \frac{4}{3} \left(\frac{8M_{H2}}{\pi RT_w} \right)^{1/2} S_v B \quad (28)$$

so that the material parameter, $S_v B$, may be calculated at each temperature from the values of n , $k_f(T_w)$ and $A(T_w)$. Again although $S_v B$ should be a constant as a function of temperature the values

calculated from Eq. (28) will probably exhibit some scatter due to experimental error. The best fit value is probably the average of the values calculated.

Deduction of the kinetic coefficients which describe $k_f(T_w)$, that is the constants k_0 , a , and E proceeds directly from the values of $k_f(T_w)$ deduced previously by obtaining the best fit values of the constants using Eq. (3). A simple regression analysis suffices for the determination of these three constants. Alternately one could plot the quantity $\ln(k_f/T_w^a)$ versus $(T_w)^{-1}$ using trial values of a until the best-fit straight line to the data is found. This defines the value of a and the intercept of the line at $(T_w)^{-1}$ equal zero is k_0 and the slope is $-E/R$.

For the special case of reaction order equal to one, a procedure similar to that just described is appropriate. In this case all the experimental data is considered in terms of $\ln(\dot{m}/P_{H2w})$ versus $(T_w)^{-1}$ and the constants k_0 , a , E , and $S_v B$ determined.

Having deduced the values of the kinetic coefficients and the material constants, a final check on the adequacy of these values is obtained by plotting the experimentally measured values of \dot{m} versus the values calculated from the right-hand-side of Eq. (7); e.g., measured \dot{m} versus predicted \dot{m} . This plot should yield a straight line of slope plus one passing through the origin and the deviation of the points from this line indicates the overall accuracy of both the experimental data and the assumed theoretical model expressed by Eq. (7).

3.4 Summary

This section has presented the data reduction technique for the Kinetics Test Cell built by SAI and currently being tested at the AFRPL. Kinetic data generated from the apparatus will be used to verify this technique. The data points recommended for the initial testing are given in Table 2.

Table 2.
RECOMMENDED DATA POINTS FOR CHECKOUT

Tw(°K)	Pw(atm)
2300	2, 5, 10, 20, 50
2700	2, 5, 10, 20, 50
2900	2, 5, 10, 20
3100	2, 5, 10, 20
3300	2, 5, 10
3500	2, 5, 10
3600	2, 5, 10, 20, 50

Modifications to the proposed data reduction technique will be determined as required as experience with the facility and the data is obtained. It should be recognized that the original intent of the experimental testing in the Kinetics Test Cell was to gain an understanding of the influence of material properties and microstructure on kinetic rate coefficients and material ablation. This objective cannot be satisfied unless data for a wide range of well-characterized materials is obtained.

Section 4
INSTALLATION OF KINETICS TEST CELL AT AFRPL

AFRPL and SAI/MSO formulated a work plan in February 1978 for delivery and installation of the kinetics test cell at AFRPL in May 1978. The plan called for AFRPL to construct an explosion proof laboratory test cave complete with power supply, gas supply, diagnostics, and external controls (see Figure 1). SAI/MSO submitted a preliminary schematic of the electrical and plumbing network to be constructed by which the kinetics test cell could be integrated to be made operable. AFRPL performed all of the facility construction but could not meet the May 1978 completion date due to prior commitment of attending personnel.

SAI/MSO delivered the kinetic test cell on 5 May 1978 and completed their portion of the installation on 15 May 1978. Final integration of the test cell in the test facility was completed 28 July 1978. At present, the apparatus is being check-out tested at the AFRPL.

Section 5

CONCLUSIONS AND RECOMMENDATIONS

Due to the delay in starting testing with the kinetics test cell at AFRPL it is premature to assess whether the experimental approach is valid for measuring kinetic reaction rates of graphites in partial pressure concentrations of selected species in propellant combustion. It is also unknown at this time whether the test cell can achieve specimen temperatures of 6000°R or greater although SAI/MSO's analysis shows that the available power is sufficient for the present test specimen configuration.

It must be recognized that this experimental approach is unique and required novel approaches to integrating resistive heating elements, test specimen, and a high pressure environment and gas flow. Since the study was a research effort, some time and experience must be gained before solutions to operational problems are evident. It was precisely this reasoning that caused SAI/MSO to adopt a design philosophy of incorporating small, low cost components which can be readily modified or replaced into an overdesigned (structural margins of safety - 10 to 66) pressure vessel.

In this study, potential difficulties of the experimental approach was assessed several times with no clear solutions to these design problems. The Aerotherm analysis (Reference 2) similarly pointed out the marginal potential of achieving true surface reaction kinetics at $T_w = 6500^{\circ}\text{R}$ and $P_{\text{H}_2} = 50$ atmospheres. However, it is evident from both the SAI/MSO and Aerotherm analysis that useful kinetic data can be derived at 50 atmospheres at temperatures of interest and SAI/MSO believes that there is a high probability of achieving kinetically affected reactions up to the design goal of $T_w = 6500^{\circ}\text{R}$ at 50 atmospheres.

SAI/MSO recommended a test matrix in Section 3.4 for determining the transition between diffusion limited and kinetically dominated regions for the delivered kinetic test cell. Another recommendation is to double the power supply for specimen

size and then assess the feasibility of enlarging the flowfield channel. The latter will require (probably) increased gas flow capabilities or ancillary pumping in order to maintain desired gas flow.

The final recommendation is to heat the test specimen in a flowing Argon environment until steady-state is reached, then through the solenoid valve arrangement of the gas feed lines, switch to the reactant gas. This eliminates the problem of rapidly heating the specimen to achieve test temperature with commensurate transient effects and thermal shock problems.

REFERENCES

1. "Behavior of Rocket Nozzle Materials at High Temperatures and Pressures of Combustion Product Gas Mixtures," Final Technical Report, Aeronutronic Publication No. 4-2413, 15 December 1963.
2. Timoshenko, Woiuowsky - Krieger, "Theory of Plates and Shells," Pg. 57, 1956.
3. "Evaluation of SAI Hot Box for Measuring Kinetic Reaction Rates of Carbon in Propellant Atmospheres," Acurex Corporation/Aerotherm Division, Aerotherm Report TM-77-192, AFRPL Contract No. F04611-76-C-0075, October 1977.
4. R. B. Dirling, Jr., D. A. Eitman, J. D. Binder, "Evaluation of Post-Test Ablation Models," Final Report AFML-TR-77-225, December 1977.
5. J. G. Baetz, "Characterization of Advanced Solid Rocket Nozzle Materials." Report SAMSO-TR-75-301, December 1975.
6. B. V. Alekseyev. "Boundary Layer and Chemical Reactions." NASA Technical Translation, TT-F-549, July 1969.
7. J. O. Hirschfelder, C. F. Curtiss, and R. B. Bird. Molecular Theory of Gases and Liquids. Wiley, New York, 1956.
8. K. M. Kratsch, L. F. Hearne, and H. R. McChesney. "Theory for the Thermophysical Performance of Charring Organic Heat-Shield Composites." LMSC-803099, 2-60-63-7, Lockheed Missiles and Space Company, Sunnyvale, California, October 1963.
9. "User's Manual, Aerotherm Graphite Surface Kinetics Computer Program." AFRPL-TR-72-23, January 1972.

A P P E N D I X A

OPERATING PROCEDURES
AND
SAFETY

FOREWORD

SAI/MSO presented to AFRPL a preliminary set of operating and safety procedures to be implemented upon initial checkout of the Kinetic Test Cell. As AFRPL performed the final integration of the test cell with ancillary laboratory power, pressure, and diagnostic controls, AFRPL has modified those instructions per their safety regulatory codes and personnel procedures. The AFRPL revised procedures are presented herein and reflect totally upon the proposed in-house research to be conducted with this facility.

TABLE OF CONTENTS

INTRODUCTION

FACILITY PREPARATION	SECTION 1
SYSTEMS CHECK.	SECTION 2
PRESSURE GAS CHECK	SECTION 3
APPARATUS PRESSURE CHECK	SECTION 4
SYSTEM PURGE	SECTION 5
TEST PROCEDURES	SECTION 6
SHUT-DOWN PROCEDURES	SECTION 7
ABORT PROCEDURES	SECTION 8

A. INTRODUCTION

Tests are an investigation of the effect various C/C material construction and processing variables have on the ablation of rocket nozzle materials. The tests have three critical areas: 1. Medium pressure (750 psi); 2. Low-medium electrical voltage (480 volts); 3. Class I propellant (Hydrogen gas).

Tests conducted under this program will provide data necessary to determine the kinetics of reaction taking place between the test material and the test gases.

Data to be obtained from the tests will be: test sample temperature, pressures apparatus inlet and outlet gas temperature, current and voltage of the power source, and the surface recession of the sample material.

Gases to be used in the tests of this program will be Hydrogen (H), Carbon Dioxide (CO₂) and water (H₂O). Inert gases to be used in the tests of this program will be Argon (AR), and gaseous nitrogen (GN₂).

The test apparatus to be used in the testing of this program is a low flow, high temperature, high pressure device. Graphite or carbon-carbon samples will be resistively heated to a maximum temperature of 6500°F at which time reactant gases will be passed across the surface of the sample at pressures up to 750 psi.

B. SCOPE

This program will be a three-year effort. A maximum of 504 tests will be conducted utilizing a variety of graphite and carbon-carbon (C/C) materials. Testing will be accomplished on a daily basis with a maximum of four tests per day.

TEST STAND DATA

GN₂ to operate regulators and asperator
Argon to purge test cell
Propellant: H₂, CO₂, H₂O

Electrical: Two (2) rectifiers producing 1000 amps
each to the test apparatus

Tests Duration: 6 seconds - 60 seconds

C. RESPONSIBILITY

It shall be the responsibility of the test engineer to insure that all test personnel are supplied with this countdown and have been briefed.

Documentation: The completion of each applicable countdown item will be checked by the test conductor (principal investigator) at the left of each item. A full countdown with all items checked will be kept in room 42, building 8451.

Prior to proceeding into the countdown, the test conductor will prepare a written list of those personnel who are members of the red crew, and designate one member on the list as the red crew leader. In addition, the individuals recognize that the designated individual is the red crew leader and that they will take their direction from him.

Any visitor, acting as an observer, will sign a visitors list. Only those persons whose names appear on the red crew list will be allowed in the red area during startup, shutdown or maintenance operations. Only those signed-in visitors escorted by a red crew member will be allowed in the area while the life test is conducted.

The red crew leader will inspect the red crew personnel prior to their entering the red area to insure that they have the required equipment and are briefed before entering the area and shall remain away from the test cell.

The names of participating personnel will be recorded below:

NAME

NAME

TEST ENGINEER/PROJECT ENGINEER
NAME

RED CREW LEADER
NAME

TEST CONDUCTOR
NAME

RED CREW MEMBER

INSTRUMENTATION TECH.

SAFETY EQUIPMENT AND BRIEFING:

- A. Safety equipment will be provided and displayed in accordance with AFR 127-101, Chapter 10, Para. 10-20, B & K.
- B. Safety training will be given in accordance with AFR 127-101, Chapter 10, Para. 10-20, B & K.
- C. The location of the safety equipment will be posted conspicuously. The emergency telephone numbers will be posted at the phones in the area of the test cell.

Section 1
FACILITY PREPARATION

Prior to the start of the testing, the following items will be accomplished:

- ___ 1.1 Test Conductor - verify HV-0-001(2500 GN2 supply to panel) is closed.
 - ___ 1.2 Test Conductor - verify Hydrogen detector meter is below ___%.
 - ___ 1.3 Red Crew - verify HV-0-003 (Argon bottle valve) is closed.
 - ___ 1.4 Red Crew - verify HV-3-004 (Hydrogen bottle valve) is closed.
 - ___ 1.5 Test Conductor - verify 440 volt breaker is open.
 - ___ 1.6 Test Conductor - turn on console on-off switch.
 - ___ 1.7 Test Conductor - push light-switch to check lights.
 - ___ 1.8 Test Conductor - check for green lights in all switches.
 - ___ 1.9 Test Conductor - reset kill switch (green light).
 - ___ 1.10 Test Conductor - verify rectifier No. 1 and No. 2 switch is off.
 - ___ 1.11 Test Conductor - cycle solenoid SV-3-001 (GH2 bottle shutoff).
 - ___ 1.12 Test Conductor - cycle solenoid SV-3-002 (test gas inlet).
 - ___ 1.13 Test Conductor - cycle solenoid SV-0-001 (Argon bottle supply).
 - ___ 1.14 Test Conductor - cycle solenoid SV-3-003 (reactant bypass).
 - ___ 1.15 Test Conductor - cycle solenoid SV-8-001 (test gas out).
- NOTE: Solenoids should be cycled only before first test of day.
- ___ 1.16 Test Conductor - verify regulator R-3-002 (test gas inlet) is closed.

- ___ 1.17 Red Crew - verify rectifier dial setting is at zero (0).
- ___ 1.18 Red Crew - inspect all electrical connections for proper connections.
- ___ 1.19 Red Crew - inspect all electrical grounds for proper connection.
- ___ 1.20 Red Crew - verify HV-0-002 (10 turn regulator) is full open.

NOTE: Authorized personnel may now work in and around the test cell. The test specimen will be installed in accordance with those procedures presented in attachment ____.

- ___ 1.21 Red Crew - verify side panels of rectifier are in place.
- ___ 1.22 Red Crew - verify rectifier intake and exhaust are not obstructed.

NOTE: Under no circumstances should the rectifier be operated if the openings at the front and rear of the rectifier are obstructed, if the fan motor is not operating or if the side panel is open, because lack of adequate forced ventilation may cause overheating and permanent damage to the rectifier.

- ___ 1.23 Red Crew - set the rectifier dials to test current ____ amps.
- ___ 1.24 Red Crew - set HV-0-002 (10-turn regulator) to ____ turns as per test request.
- ___ 1.25 Red Crew - open HV-0-003 (Argon bottle valve).
- ___ 1.26 Red Crew - open HV-3-004 (Hydrogen bottle valve).

Section 2
SYSTEMS CHECK

NOTE: Only authorized personnel will be in the local area of test cell No. 4 when H2 is in use.

- ___ 2.1 Red Crew - secure southwest gate and chain to parking lot area at rear of test cell.
- ___ 2.2 Red Crew - secure all doors into the test cell area.
- ___ 2.3 Test Conductor - place the area in red and notify the safety operations center (32632).

Section 3
PRESSURE CHECK AND PURGE OF HYDROGEN SYSTEM

- ___ 3.1 Test Conductor - open HV-0-001 (2500 GN2 supply to panel).
- ___ 3.2 Test Conductor - verify regulator R-3-002 (test gas inlet) closed.
- ___ 3.3 Test Conductor - close solenoid SV-0-001 (Argon bottle supply).
- ___ 3.4 Test Conductor - close solenoid SV-8-001 (test gas out).
- ___ 3.5 Test Conductor - open solenoid SV-3-001 (GH2 bottle shutoff). 2030
- ___ 3.6 INSTRUMENTATION - START RECORDERS
- ___ 3.7 Test Conductor - pressurize regulator R-3-001 (GH2 supply) to ___ psi as per test request and verify pressure on transducer channel ___.
- ___ 3.8 Test Conductor - close solenoid SV-3-001, (GH2 bottle shutoff).
- ___ 3.9 Test Conductor - wait 60 seconds, then verify pressure on transducer channel no. ___ (GH2 supply).
- ___ 3.10 Test Conductor - open solenoid SV-3-001 (GH2 bottle shutoff).
- ___ 3.11 Test Conductor - open regulator R-0-003 (aspirator GN2 supply) to ___ psi as per test request: verify.

- ___ 3.12 Test Conductor - open solenoid SV-3-002 (reactant test gas).
- ___ 3.13 Test Conductor - open solenoid SV-3-003 (reactant by-pass) for ___ seconds.
- ___ 3.14 Test Conductor - close solenoid SV-3-002 (reactant test gas).
- ___ 3.15 Test Conductor - close solenoid SV-3-003 (reactant by-pass).
- ___ 3.16 Test Conductor - close regulator R-0-003 (aspirator GN2 supply).

Section 4 APPARATUS PRESSURE CHECK

- ___ 4.1 Test Conductor - open regulator R-0-001 (Argon supply) to 750 psi: Verify.
- ___ 4.2 Test Conductor - open solenoid SV-0-001 (Argon bottle supply).
- ___ 4.3 Test Conductor - open regulator R-3-002 (test gas inlet); verify apparatus pressure at 750 psi.
- ___ 4.4 Test Conductor - close regulator R-0-001 (Argon supply).
- ___ 4.5 Instrumentation - wait 60 seconds, then verify apparatus pressure at 750 psi on panel gauge 002.

Section 5 SYSTEM PURGE

- ___ 5.1 Test Conductor - open solenoid SV-8-001 (test gas out) and wait ___ seconds.
- ___ 5.2 Test Conductor - close solenoid SV-8-001 (test gas out).
- ___ 5.3 Test Conductor - open regulators R-0-001 (Argon supply) to ___ psi as per test request: Verify.

Section 6
TEST PROCEDURES

NOTE: Should structure failure of apparatus occur, go to Abort 2440 Procedure No. 1.

Should specimen temperature exceed ____°F, go to Abort Procedure No. 2.

Should a rapid depressurization of flow field occur, go to Abort Procedure No. 2.

Should a fire or explosion within the test cell occur go to Abort Procedure No. 3.

- ____ 6.1 Test Conductor - close 440 vac breakers.
- ____ 6.2 Test Conductor - open regulator R-0-003 (aspirator GN2 supply) to ____ psi as per test request: Verify.
- ____ 6.3 Test Conductor - open solenoid SV-8-001 (test gas out) and simultaneously turn on rectifier No. 1 switch.
- ____ 6.4 Instrumentation - monitor pyrometer reading and inform the test conductor when the temperature is ____°F as per test request.

NOTE: The test conductor should be informed immediately since 2710 time is a test factor. Instrumentation will continue to monitor the test specimen temperature and inform the test conductor when the temperature exceeds ____°F.

- ____ 6.5 Test Conductor - simultaneously close solenoid SV-0-001 (Argon bottle supply) and open solenoid SV-3-002 (open reactant test gas).
- ____ 6.6 Test Conductor - after ____ seconds, simultaneously close solenoid SV-3-001 (GH2 bottle shutoff) and open solenoid SV-0-001 (Argon bottle supply).
- ____ 6.7 Test Conductor - turn off rectifier 1 (and rectifier 2) switch.
- ____ 6.8 Test Conductor - after ____ seconds, close solenoid regulator R-0-001 (Argon supply).

Section 7
SHUT-DOWN PROCEDURES

NOTE: Before entering the cell, the following procedures must be accomplished.

- ___ 7.1 Test Conductor - open 440 volt breakers
- ___ 7.2 Test Conductor - close regulator R-0-003 (aspirator GN2 supply).
- ___ 7.3 Instrumentation - turn off recorders.

NOTE: The Red Crew may enter the test cell.

- ___ 7.4 Red Crew - return rectifier dial to zero (0) setting.
- ___ 7.5 Red Crew - close HV-0-003 (Argon bottle valve).
- ___ 7.6 Red Crew - close HV-3-004 (Hydrogen bottle valve).
2900.
- ___ 7.7 Test Conductor - place area in amber condition and notify
- ___ 7.8 Test Conductor - place area in amber condition and notify the safety operations center after last test of day (32632).

NOTE: Warning - Apparatus is very hot and can cause severe burns. Use caution when working around the apparatus after a test. Apparatus should be allowed to cool to ___°F. Removal of the sample will be done in accordance with Appendix 2.

- ___ 7.9 Red Crew - verify HV-0-002 (ten-turn regulator to the full open position.
- ___ 7.10 Test Conductor - turn console voltage off.
- ___ 7.11 Test Conductor - close HV-0-001 (2500 psi GN2 supply to console).

Section 8
ABORT PROCEDURES

ABORT PROCEDURE NO. 1

- ___ 8.1 Test Conductor - activate emergency kill switch.
- ___ 8.2 Test Conductor - close R-3-001 (GH2 supply) and R-0-001 (Argon supply).
- ___ 8.3 Test Conductor - after 5 minutes close R-0-003 (aspirator GN2 supply).
- ___ 8.4 Instrumentation - turn off recorders.
- ___ 8.5 Test Conductor - proceed with shut-down procedures, Section 7.

ABORT PROCEDURE NO. 2

- ___ 8.6 Test Conductor - activate emergency kill switch.
- ___ 8.7 Test Conductor - close R-3-001 (GH2 supply).
- ___ 8.8 Test Conductor - after 2 minutes close R-0-001 (Argon supply) and R-0-003 (aspirator GN2 supply).
- ___ 8.9 Instrumentation - turn off recorders.
- ___ 8.10 Test Conductor - proceed with shutdown procedures, Section 7.

ABORT PROCEDURE NO. 3

- ___ 8.11 Test Conductor - activate emergency kill switch.
- ___ 8.12 Test Conductor - close R-3-001 (GH2 supply).
- ___ 8.13 Test Conductor - notify fire department (117).

TABLE OF CONTENTS

<u>Section</u>		<u>Page</u>
1	INTRODUCTION AND SUMMARY	3
2	DESIGN STUDY AND FABRICATION OF A KINETIC TEST CELL	5
	2.1 Flowfield Consideration	7
	2.1.1 Heterogeneous Reactions	7
	2.1.2 Experimental Approach	9
	2.2 Experimental Kinetic Test Cell Design	10
	2.3 Analysis of Kinetics Test Cell Design	19
	2.3.1 Thermal Analysis	20
	2.3.2 Surface Kinetics and Flowfield Size Analysis	22
	2.4 Fabrication	24
	2.4.1 Checkout Runs	26
	2.4.2 Test Facility Layout Recommendation	26
3	HETEROGENEOUS MATERIAL KINETIC DATA REDUCTIONS	28
	3.1 Test Data Acquisition	28
	3.2 Reactions Kinetics	31
	3.3 Test Data Reduction	38
	3.4 Summary	40
4	INSTALLATION OF KINETICS TEST CELL AT AFRPL	42
5	CONCLUSIONS AND RECOMMENDATIONS	43
6	APPENDIX A OPERATING PROCEDURES AND SAFETY	A-47

Accession For	
NTIS GRA&I	<input checked="checked" type="checkbox"/>
DDC TAB	<input type="checkbox"/>
Unannounced	<input type="checkbox"/>
Justification	
By _____	
Distribution/_____	
Availability Codes	
Dist	Avail and/or special
A	